

Revealing Hidden Substructures in the M_{BH} - σ Diagram, and Refining the Bend in the L - σ Relation

NANDINI SAHU,^{1,2} ALISTER W. GRAHAM² AND BENJAMIN L. DAVIS²

¹*OzGrav-Swinburne, Centre for Astrophysics and Supercomputing, Swinburne University of Technology, Hawthorn, VIC 3122, Australia*

²*Centre for Astrophysics and Supercomputing, Swinburne University of Technology, Hawthorn, VIC 3122, Australia*

Submitted to ApJ

ABSTRACT

Using 143 early- and late-type galaxies (ETGs and LTGs) with directly-measured super-massive black hole masses (M_{BH}), we build upon our previous discoveries that: (i) LTGs, most of which have been alleged to contain a pseudobulge, follow the relation $M_{BH} \propto M_{*,sph}^{2.16 \pm 0.32}$; and (ii) the ETG relation $M_{BH} \propto M_{*,sph}^{1.27 \pm 0.07}$ is an artifact of ETGs with/without disks following parallel $M_{BH} \propto M_{*,sph}^{1.9 \pm 0.2}$ relations which are offset by an order of magnitude in the M_{BH} -direction. Here we searched for substructure in the M_{BH} -(central velocity dispersion, σ) diagram using our recently published, multi-component, galaxy decompositions; investigating divisions based on the presence of a depleted stellar core (major dry-merger), a disk (minor wet/dry-merger, gas accretion), or a bar (evolved unstable disk). The Sérsic and core-Sérsic galaxies define two distinct relations: $M_{BH} \propto \sigma^{5.86 \pm 0.33}$ and $M_{BH} \propto \sigma^{8.54 \pm 1.07}$, with $\Delta_{rms|BH} = 0.51$ and 0.47 dex, respectively. We also report on the consistency with the slopes and bends in the galaxy luminosity (L)- σ relation due to Sérsic and core-Sérsic ETGs, and LTGs which all have Sérsic light-profiles. The bend in the M_{BH} - σ diagram (superficially) reappears upon separating galaxies with/without a disk, while we find no significant offset between barred and non-barred galaxies, nor between galaxies with/without active galactic nuclei. We also address selection biases purported to affect the scaling relations for dynamically-measured M_{BH} samples. These new, type-dependent, M_{BH} - σ relations more precisely estimate M_{BH} in other galaxies, and hold implications for galaxy/black hole co-evolution theories, simulations, feedback, the pursuit of a black hole fundamental plane, and calibration of virial f -factors for reverberation-mapping.

Keywords: black hole physics — galaxies: evolution — galaxies: kinematics and dynamics — galaxies: elliptical and lenticular, cD — galaxies: spiral — galaxies: structure

1. INTRODUCTION

The first observational works on the correlation between central black hole mass (M_{BH}) and the stellar velocity dispersion (σ) of a galaxy (Ferrarese & Merritt 2000; Gebhardt et al. 2000) revealed a relation with little or no intrinsic scatter, suggesting that the M_{BH} - σ relation could be the most fundamental of the black hole scaling relations. However, surprisingly, the slopes reported by the two studies were not in agreement and supported two competing feedback models be-

tween the Super-Massive Black Holes (SMBHs) and their host galactic bulges. Ferrarese & Merritt (2000) found $M_{BH} \propto \sigma^{4.80 \pm 0.50}$, which supported the prediction $M_{BH} \propto \sigma^5$ based on the energy-balancing feedback model of Silk & Rees (1998). Gebhardt et al. (2000) reported $M_{BH} \propto \sigma^{3.75 \pm 0.30}$, supporting the feedback model of Fabian (1999) based upon momentum conservation, which predicted $M_{BH} \propto \sigma^4$.

Merritt & Ferrarese (2001) later revealed that Gebhardt et al. (2000) had found a shallower slope due to the asymmetric linear regression routine that Gebhardt et al. (2000) employed — which ignored the

measurement errors in the velocity dispersion¹ — plus Gebhardt et al.’s relation was biased by the low-velocity dispersion which they had used for the Milky Way. Gebhardt et al. (2000) effectively solved the “Observer’s Questions” while Ferrarese & Merritt (2000) effectively had answered the “Theorist’s Question,” as was later posed by Novak et al. (2006). The reason behind obtaining almost zero intrinsic scatter in the $M_{BH}-\sigma$ relation was possibly the small sample size, or perhaps Ferrarese & Merritt (2000) had a “gold standard” of reliable black hole masses with well-resolved spheres-of-influence (Ferrarese & Ford 2005). Subsequent works on larger galaxy samples have found a non-zero intrinsic scatter.

With an increase in the number of barred galaxies with directly measured SMBH masses, some studies (Graham 2007, 2008a,b; Hu 2008) found that barred galaxies have a tendency to be offset, from the $M_{BH}-\sigma$ relation, towards higher σ or lower M_{BH} , suggesting that the inclusion of barred galaxies may produce a steeper relation with larger scatter (Graham et al. 2011; Graham & Scott 2013). Hu (2008) claimed that all the offset galaxies in their sample had “pseudo-bulges²” with low-mass black holes, while according to Graham (2008b), the offset could be either because of a low M_{BH} in pseudo-bulges or the elevated velocity dispersions in barred galaxies. Supporting the latter possibility, the simulation by Hartmann et al. (2014) suggested that bars may cause increased velocity dispersion in galactic bulges whether they are classical or pseudo-bulges (see also Brown et al. 2013). Interestingly, the recent observational work by Sahu et al. (2019) found that barred galaxies are not offset in the black hole mass versus galaxy stellar mass ($M_{*,gal}$) diagram, nor in the black hole mass versus spheroid/bulge stellar mass ($M_{*,sph}$) diagram, eliminating under-massive black holes as the reason behind the apparent offset in the $M_{BH}-\sigma$ diagram and strengthening the prospect of barred galaxies having an increased velocity dispersion. However, as the number of barred galaxies in Sahu et al. (2019) is still quite small, this interpretation may require further confirmation.

In addition to the reported substructure in the $M_{BH}-\sigma$ diagram due to barred galaxies, some studies

(e.g., McConnell & Ma 2013) have noticed that massive galaxies are offset towards the high- M_{BH} side at the high-mass end of their $M_{BH}-\sigma$ relation. These galaxies are mostly Brightest Cluster Galaxies (BCGs) or Central Cluster Galaxies (CCGs) which are considered to be a product of multiple dry mergers. Galaxies which have undergone dry mergers can have a deficit of light at their centers because the binary SMBHs from the two merging galaxies scour out the stars from the center of the merged galaxy through the transfer of their orbital angular momentum (Begelman et al. 1980). Such galaxies with a (partially) depleted core were discovered by King & Minkowski (1966, 1972) and are referred to as core-Sérsic (Graham et al. 2003) galaxies due to their flattened core relative to the inward extrapolation of their bulge’s outer Sérsic (Sérsic 1963) light profile. Galaxies which grow over time via accretion or gas-rich mergers are likely to have bulges with Sérsic light-profiles. Contrary to McConnell & Ma (2013), the recent work by Savorgnan & Graham (2015) claimed that Sérsic and core-Sérsic galaxies broadly follow the same $M_{BH}-\sigma$ relation, and so was the case with slow and fast rotating galaxies in their sample. Thus, still, debates over the substructures in the $M_{BH}-\sigma$ diagram due to barred and non-barred galaxies, Sérsic and core-Sérsic galaxies, and fast and slow rotating galaxies (galaxies with and without a rotating disk) persist.

Using the hitherto largest sample of 143 galaxies, comprised of all Early-Type Galaxies (ETGs) and Late-Type Galaxies (LTGs) with directly measured SMBH masses, our work investigates the underlying relationship between black hole mass and central velocity dispersion for various sub-classes of the host galaxy. We classify these galaxies into Sérsic, core-Sérsic, barred, non-barred, and galaxies with and without a disk, based on our detailed multi-component decompositions (coupled with kinematical information) presented in Davis et al. (2019) and Sahu et al. (2019), and also into galaxies with and without an Active Galactic Nucleus (AGN) identified using the catalog of Véron-Cetty & Véron (2010).

We endeavor here to build upon our recent revelation that ETGs follow $M_{BH} \propto M_{*,sph}^{1.27 \pm 0.07}$ (Sahu et al. 2019, their Equation 10). However, we showed in Sahu et al. (2019, see their Figure 8) that this single relation for ETGs is misleading because we found that ETGs with and without a disk define two separate (parallel) $M_{BH} \propto M_{*,sph}^{1.9 \pm 0.2}$ relations which are offset by more than an order of magnitude (1.12 dex) in the M_{BH} -direction. This paradigm shifting discovery provided the impetus for us to now investigate for similar substructure in the $M_{BH}-\sigma$ relation.

¹ Tremaine et al. (2002) also used an asymmetric linear regression, ignoring the intrinsic scatter in the velocity dispersion direction (see Novak et al. 2006; Graham 2016, see his section titled “slippery slopes”).

² Pseudo-bulges are not only difficult to identify Graham (2014), but Graham (2019) explains why diagrams using “effective” half-light parameters cannot identify pseudobulges.

In order to provide a consistency check between the various scaling relations, this paper also establishes the galaxy luminosity (L)- σ relation for our ($3.6\mu\text{m}$) ETG sample, and for an updated V-band data-set (Lauer et al. 2007). We reveal the apparent bend in the ETG $L-\sigma$ relation from both data-sets, which has been observed in other wavelength bands (e.g., Matković & Guzmán 2005; de Rijcke et al. 2005; Lauer et al. 2007; Graham & Soria 2019). Additionally, we show the behavior of LTGs (spirals), with directly measured black hole masses, in the $L-\sigma$ diagram. We mate these $L-\sigma$ relations with those in the $M_{BH}-\sigma$ diagram to reveal the consistency between the scaling relations.

Section 2 describes our data-set and the galaxy exclusions applied, along with the reasons for this. In Section 3, we briefly discuss the method of linear regression that we have used to establish our scaling relations, and we further present the new $M_{BH}-\sigma$ relations that we have found for the various categories based on the morphological classes mentioned above. This is accompanied by discussions on the behavior of the $M_{BH}-\sigma$ relations for each category. In Section 4, we check on the internal consistency between our $M_{BH}-\sigma$ relations and the latest $M_{BH}-M_{*,gal}$ (and $M_{BH}-M_{*,sph}$) relations, while Section 5 presents our bent $L-\sigma$ relations, along with a review of previous works based on different wavelength bands. Section 6 addresses a much-discussed selection bias regarding the spatial-resolution of the gravitational sphere-of-influence of the black holes, and it also investigates the previously observed offset between galaxies with a dynamically measured black hole mass and galaxies without a dynamically measured black hole mass in the $\sigma-M_{*,gal}$ diagram (Shankar et al. 2016). This is followed by a discussion of the implications of our scaling relations and the main conclusions of our work summarized in Section 7.

2. DATA

We have compiled the largest sample to date of 143 galaxies with directly measured super-massive black hole masses obtained using direct imaging, stellar dynamics, gas dynamics, or kinematics of megamasers. This sample is comprised of 94 early-type and 49 late-type galaxies. The data for 84 ETGs comes from the recent works by Sahu et al. (2019) and Savorgnan et al. (2016). These 84 ETGs have been used in Sahu et al.

(2019) to establish hitherto the strongest $M_{BH}-M_{*,sph}$ and $M_{BH}-M_{*,gal}$ relations for ETGs, based on the bulge and total galaxy stellar masses measured using state-of-the-art isophotal modelling and multi-component decompositions of predominantly Near Infra-Red (NIR) images.

For the remaining 10 ETGs, data for one galaxy comes from Nowak et al. (2007), which measured M_{BH} using stellar dynamics, while the data for the remaining nine ETGs is taken from recent papers. Out of these nine, two ETGs are from Nguyen et al. (2018) and six ETGs come from Thater et al. (2019), where both the works measured M_{BH} using stellar dynamics, and the data for the last ETG is taken from Boizelle et al. (2019) which presents M_{BH} obtained using gas dynamics.

Data for 44 of the 49 LTGs (spiral galaxies) is taken from Davis et al. (2018) and Davis et al. (2019), where they also present the $M_{BH}-M_{*,sph}$, $M_{BH}-M_{*,disk}$, and $M_{BH}-M_{*,gal}$ relations for spiral galaxies based on predominantly NIR imaging and multi-component decomposition. Out of the remaining LTGs, four are taken from Combes et al. (2019), and one from Nguyen et al. (2019), where the central SMBH masses have been measured using gas dynamics.

Our total galaxy sample is listed in Table 1, which includes information on the galaxy type, distance, updated morphology, presence of a bar, disk, core, AGN, M_{BH} , and reference, plus the central stellar velocity dispersion. The velocity dispersions for the majority of our galaxies are taken from the HYPERLEDA database (Paturel et al. 2003), as of February 2019. The velocity dispersion values provided on HYPERLEDA are homogenised for a uniform aperture size of $\lesssim 0.6$ kpc. Galaxies for which we obtained velocity dispersions from other sources are indicated in Table 1. The morphologies reflect the presence, or not, of an intermediate or large-scale disk, and also bar, with types designated by the morphological galaxy classification grid given by Graham (2019).

For the majority of galaxies in our sample, the uncertainty in velocity dispersion reported by HYPERLEDA is minimal, $\lesssim 10\%$. Given that seeing and slit orientation can influence the measured velocity dispersion, we use a constant uncertainty of 10%, whereas for M_{BH} , we use the errors provided by the sources, listed in Table 1.

Table 1. Galaxy Sample

Galaxy	Type	Distance	Morph	Bar	Disk	Core	AGN	$\log(M_{BH}/M_{\odot})$	Source	$\log(\sigma/\text{km s}^{-1})$
		(Mpc)						(dex)		(dex)
(1)	(2)	(3)	(4)	(5)	(6)	(7)	(8)	(9)	(10)	(11)
IC 1459	ETG	28.4	E	nb	no	yes	yes	9.38 ± 0.20	SG(2016)	2.47
NGC 0821	ETG	23.4	E	nb	no	no	no	7.59 ± 0.17	SG(2016)	2.30
NGC 1023	ETG	11.1	S0-bar	b	yes	no	no	7.62 ± 0.05	SG(2016)	2.29
NGC 1316	ETG	18.6	merger	nb	yes	no	no	8.18 ± 0.26	SG(2016)	2.35
NGC 1332	ETG	22.3	ES	nb	yes	no	no	9.16 ± 0.07	SG(2016)	2.47
NGC 1399	ETG	19.4	E	nb	no	yes	no	8.67 ± 0.06	SG(2016)	2.52
NGC 2549	ETG	12.3	S0	b	yes	no	no	7.15 ± 0.60	SG(2016)	2.15
NGC 2778	ETG	22.3	S0	b	yes	no	no	7.18 ± 0.34	SG(2016)	2.19
NGC 3091	ETG	51.2	E	nb	no	yes	no	9.56 ± 0.04	SG(2016)	2.49
NGC 3115	ETG	9.4	S0	nb	yes	no	no	8.94 ± 0.25	SG(2016)	2.42
NGC 3245	ETG	20.3	S0	b	yes	no	no	8.30 ± 0.12	SG(2016)	2.32
NGC 3377	ETG	10.9	E	nb	no	no	no	7.89 ± 0.04	SG(2016)	2.13
NGC 3379 (M 105)	ETG	10.3	E	nb	no	yes	no	8.60 ± 0.12	SG(2016)	2.31
NGC 3384	ETG	11.3	S0	b	yes	no	no	7.23 ± 0.05	SG(2016)	2.16
NGC 3414	ETG	24.5	E	nb	no	no	no	8.38 ± 0.06	SG(2016)	2.38
NGC 3489	ETG	11.7	S0	b	yes	no	no	6.76 ± 0.07	SG(2016)	2.02
NGC 3585	ETG	19.5	E	nb	no	no	no	8.49 ± 0.13	SG(2016)	2.33
NGC 3607	ETG	22.2	E	nb	no	no	yes	8.11 ± 0.18	SG(2016)	2.35
NGC 3608	ETG	22.3	E	nb	no	yes	no	8.30 ± 0.18	SG(2016)	2.29
NGC 3842	ETG	98.4	E	nb	no	yes	no	9.99 ± 0.13	SG(2016)	2.49
NGC 3998	ETG	13.7	S0	b	yes	no	yes	8.91 ± 0.11	SG(2016)	2.42
NGC 4261	ETG	30.8	E	nb	no	yes	yes	8.70 ± 0.09	SG(2016)	2.47
NGC 4291	ETG	25.5	E	nb	no	yes	no	8.52 ± 0.36	SG(2016)	2.47
NGC 4374 (M 84)	ETG	17.9	E	nb	no	yes	yes	8.95 ± 0.05	SG(2016)	2.44
NGC 4459	ETG	15.7	S0	nb	yes	no	no	7.83 ± 0.09	SG(2016)	2.24
NGC 4472 (M 49)	ETG	17.1	E	nb	no	yes	yes	9.40 ± 0.05	SG(2016)	2.45
NGC 4473	ETG	15.3	E	nb	no	no	no	8.08 ± 0.36	SG(2016)	2.25
NGC 4486 (M 87)	ETG	16.8	E	nb	no	yes	yes	9.81 ± 0.05^a	SG(2016)	2.51
NGC 4564	ETG	14.6	S0	nb	yes	no	no	7.78 ± 0.06	SG(2016)	2.19
NGC 4596	ETG	17.0	S0	b	yes	no	no	7.90 ± 0.20	SG(2016)	2.15
NGC 4621 (M 59)	ETG	17.8	E	nb	no	no	no	8.59 ± 0.05	SG(2016)	2.36
NGC 4697	ETG	11.4	E	nb	no	no	no	8.26 ± 0.05	SG(2016)	2.22
NGC 4889	ETG	103.2	E	nb	no	yes	no	10.32 ± 0.44	SG(2016)	2.59
NGC 5077	ETG	41.2	E	nb	no	yes	yes	8.87 ± 0.22	SG(2016)	2.40
NGC 5128	ETG	3.8	merger	nb	yes	no	no	7.65 ± 0.13	SG(2016)	2.01
NGC 5576	ETG	24.8	E	nb	no	no	no	8.20 ± 0.10	SG(2016)	2.26
NGC 5846	ETG	24.2	E	nb	no	yes	no	9.04 ± 0.05	SG(2016)	2.38
NGC 6251	ETG	104.6	E	nb	no	yes	yes	8.77 ± 0.16	SG(2016)	2.49
NGC 7619	ETG	51.5	E	nb	no	yes	no	9.40 ± 0.09	SG(2016)	2.50
NGC 7768	ETG	112.8	E	nb	no	yes	no	9.11 ± 0.15	SG(2016)	2.46
NGC 1271	ETG	80.0	ES	nb	yes	no	no	9.48 ± 0.16	GCS(2016)	2.44 [11a]
NGC 1277	ETG	72.5	ES	nb	yes	no	no	9.08 ± 0.12	G+7(2016)	2.48 [11b]
A1836 BCG	ETG	158.0	E	nb	no	yes	no	9.59 ± 0.06	SGD(2019)	2.49[11c]
A3565 BCG (IC 4296)	ETG	40.7	E	nb	no	no	yes	9.04 ± 0.09	SGD(2019)	2.52
Mrk 1216	ETG	94.0	S0	nb	yes	no	yes	9.69 ± 0.16	SGD(2019)	2.51
NGC 0307	ETG	52.8	SAB0	b	yes	no	no	8.34 ± 0.13	SGD(2019)	2.43
NGC 0404	ETG	3.1	S0	nb	yes	no	no	4.85 ± 0.13	SGD(2019)	1.54
NGC 0524	ETG	23.3	SA0(rs)	nb	yes	yes	no	8.92 ± 0.10	SGD(2019)	2.37
NGC 1194	ETG	53.2	S0	nb	yes	no	yes	7.81 ± 0.04	SGD(2019)	2.17 [11d]
NGC 1275	ETG	72.9	E	nb	no	no	yes	8.90 ± 0.20	SGD(2019)	2.39
NGC 1374	ETG	19.2	S0	nb	yes	no	no	8.76 ± 0.05	SGD(2019)	2.25

Table 1 continued

Table 1 (*continued*)

Galaxy	Type	Distance	Morph	Bar	Disk	Core	AGN	$\log(M_{BH}/M_{\odot})$	Source	$\log(\sigma/\text{km s}^{-1})$
(1)	(2)	(3)	(4)	(5)	(6)	(7)	(8)	(9)	(10)	(11)
NGC 1407	ETG	28.0	E	nb	no	yes	no	9.65 ± 0.08	SGD(2019)	2.42
NGC 1550	ETG	51.6	E	nb	no	yes	no	9.57 ± 0.06	SGD(2019)	2.48
NGC 1600	ETG	64.0	E	nb	no	yes	no	10.23 ± 0.05	SGD(2019)	2.52
NGC 2787	ETG	7.3	SB0(r)	b	yes	no	yes	7.60 ± 0.06	SGD(2019)	2.28
NGC 3665	ETG	34.7	S0	nb	yes	no	no	8.76 ± 0.10	SGD(2019)	2.33
NGC 3923	ETG	20.9	E	nb	no	yes	no	9.45 ± 0.13	SGD(2019)	2.39
NGC 4026	ETG	13.2	SB0	b	yes	no	no	8.26 ± 0.11	SGD(2019)	2.24
NGC 4339	ETG	16.0	S0	nb	yes	no	no	7.63 ± 0.33	SGD(2019)	2.05
NGC 4342	ETG	23.0	ES	nb	yes	no	no	8.65 ± 0.18	SGD(2019)	2.38
NGC 4350	ETG	16.8	EBS	b	yes	no	no	8.86 ± 0.41	SGD(2019)	2.26
NGC 4371	ETG	16.9	SB(r)0	b	yes	no	no	6.85 ± 0.08	SGD(2019)	2.11
NGC 4429	ETG	16.5	SB(r)0	b	yes	no	no	8.18 ± 0.09	SGD(2019)	2.24
NGC 4434	ETG	22.4	S0	nb	yes	no	no	7.85 ± 0.17	SGD(2019)	2.07
NGC 4486B	ETG	15.3	E	nb	no	no	no	8.76 ± 0.24	SGD(2019)	2.22
NGC 4526	ETG	16.9	S0	nb	yes	no	no	8.67 ± 0.05	SGD(2019)	2.35
NGC 4552	ETG	14.9	E	nb	no	no	yes	8.67 ± 0.05	SGD(2019)	2.40
NGC 4578	ETG	16.3	S0(r)	nb	yes	no	no	7.28 ± 0.35	SGD(2019)	2.05
NGC 4649	ETG	16.4	E	nb	no	yes	no	9.67 ± 0.10	SGD(2019)	2.52
NGC 4742	ETG	15.5	S0	nb	yes	no	no	7.15 ± 0.18	SGD(2019)	2.01
NGC 4751	ETG	26.9	S0	nb	yes	yes	no	9.15 ± 0.05	SGD(2019)	2.54
NGC 4762	ETG	22.6	SB0	b	yes	no	no	7.36 ± 0.15	SGD(2019)	2.15
NGC 5018	ETG	40.6	S0	nb	yes	no	no	8.02 ± 0.09	SGD(2019)	2.33
NGC 5252	ETG	96.8	S0	nb	yes	no	yes	9.00 ± 0.40	SGD(2019)	2.27
NGC 5328	ETG	64.1	E	nb	no	yes	no	9.67 ± 0.15	SGD(2019)	2.50
NGC 5419	ETG	56.2	E	nb	no	yes	no	9.86 ± 0.14	SGD(2019)	2.54
NGC 5516	ETG	58.4	E	nb	no	yes	no	9.52 ± 0.06	SGD(2019)	2.49
NGC 5813	ETG	31.3	S0	nb	yes	yes	no	8.83 ± 0.06	SGD(2019)	2.37
NGC 5845	ETG	25.2	ES	nb	yes	no	no	8.41 ± 0.22	SGD(2019)	2.36
NGC 6086	ETG	138.0	E	nb	no	yes	no	9.57 ± 0.17	SGD(2019)	2.51
NGC 6861	ETG	27.3	ES	nb	yes	no	no	9.30 ± 0.08	SGD(2019)	2.57
NGC 7052	ETG	66.4	E	nb	no	yes	no	8.57 ± 0.23	SGD(2019)	2.45
NGC 7332	ETG	24.9	SB0	b	yes	no	no	7.11 ± 0.20	SGD(2019)	2.11
NGC 7457	ETG	14.0	S0	nb	yes	no	no	7.00 ± 0.30	SGD(2019)	1.83
NGC 4486A	ETG	13.9	E	nb	no	no	no	7.10 ± 0.32	No+7(2007)	2.12
NGC 5102	ETG	3.2	S0	nb	yes	no	no	5.94 ± 0.38	Ngu+10(2018)	1.79
NGC 5206	ETG	3.5	dE/dS0	nb	no?	no	no	5.67 ± 0.36	Ngu+10(2018)	1.62
NGC 0584	ETG	19.1	S0	nb	yes	yes	no	8.11 ± 0.18	Th+6(2019)	2.33 [11e]
NGC 2784	ETG	9.6	S0	nb	yes	no	no	8.00 ± 0.31	Th+6(2019)	2.39 [11e]
NGC 3640	ETG	26.3	E	nb	no	yes	no	7.89 ± 0.34	Th+6(2019)	2.24 [11e]
NGC 4281	ETG	24.4	S0	nb	yes	no	no	8.73 ± 0.08	Th+6(2019)	2.50 [11e]
NGC 4570	ETG	17.1	S0	nb	yes	no	no	7.83 ± 0.14	Th+6(2019)	2.32 [11e]
NGC 7049	ETG	29.9	S0	nb	yes	no	no	8.51 ± 0.12	Th+6(2019)	2.42 [11e]
NGC 3258	ETG	31.3	E	nb	no	yes	no	9.35 ± 0.05	Bo+7(2019)	2.41
Circinus	LTG	4.2	SABb	nb	yes	no	yes	6.25 ± 0.11	DGC(2019)	2.17
Cygnus A	LTG	258.8	S	nb	yes	no	yes	9.44 ± 0.13	DGC(2019)	2.43 [11f]
ESO558-G009	LTG	115.4	Sbc	nb	yes	no	no	7.26 ± 0.04	DGC(2019)	2.23 [11g]
IC 2560	LTG	31.0	SBb	b	yes	no	yes	6.49 ± 0.20	DGC(2019)	2.14
J0437+2456	LTG	72.8	SB	b	yes	no	no	6.51 ± 0.05	DGC(2019)	2.04 [11g]
Milky Way	LTG	7.9	SBbc	b	yes	no	no	6.60 ± 0.02	DGC(2019)	2.02 [11f]
Mrk 1029	LTG	136.9	S	nb	yes	no	no	6.33 ± 0.12	DGC(2019)	2.12 [11g]
NGC 0224	LTG	0.8	SBb	b	yes	no	no	8.15 ± 0.16	DGC(2019)	2.19

Table 1 *continued*

Table 1 (*continued*)

Galaxy	Type	Distance	Morph	Bar	Disk	Core	AGN	$\log(M_{BH}/M_{\odot})$	Source	$\log(\sigma/\text{km s}^{-1})$
(1)	(2)	(3)	(4)	(5)	(6)	(7)	(8)	(9)	(10)	(11)
NGC 0253	LTG	3.5	SABc	b	yes	no	no	7.00 ± 0.30	DGC(2019)	1.98
NGC 1068	LTG	10.1	SBb	b	yes	no	yes	6.75 ± 0.08	DGC(2019)	2.21
NGC 1097	LTG	24.9	SBb	b	yes	no	yes	8.38 ± 0.04	DGC(2019)	2.29 [11h]
NGC 1300	LTG	14.5	SBbc	b	yes	no	no	7.71 ± 0.16	DGC(2019)	2.34
NGC 1320	LTG	37.7	Sa	nb	yes	no	no	6.78 ± 0.29	DGC(2019)	2.04
NGC 1398	LTG	24.8	SBab	b	yes	no	no	8.03 ± 0.11	DGC(2019)	2.29
NGC 2273	LTG	31.6	SBa	b	yes	no	no	6.97 ± 0.09	DGC(2019)	2.15
NGC 2748	LTG	18.2	Sbc	nb	yes	no	no	7.54 ± 0.21	DGC(2019)	1.98
NGC 2960	LTG	71.1	Sa	nb	yes	no	no	7.06 ± 0.17	DGC(2019)	2.22 [11i]
NGC 2974	LTG	21.5	SB	b	yes	no	yes	8.23 ± 0.07	DGC(2019)	2.37
NGC 3031	LTG	3.5	SABab	nb	yes	no	no	7.83 ± 0.09	DGC(2019)	2.18
NGC 3079	LTG	16.5	SBcd	b	yes	no	yes	6.38 ± 0.12	DGC(2019)	2.24
NGC 3227	LTG	21.1	SABa	b	yes	no	yes	7.88 ± 0.14	DGC(2019)	2.10
NGC 3368	LTG	10.7	SABa	b	yes	no	no	6.89 ± 0.09	DGC(2019)	2.07
NGC 3393	LTG	55.8	SBa	b	yes	no	yes	7.49 ± 0.05	DGC(2019)	2.30
NGC 3627	LTG	10.6	SBb	b	yes	no	yes	6.95 ± 0.05	DGC(2019)	2.10
NGC 4151	LTG	19.0	SABa	b	yes	no	yes	7.68 ± 0.37	DGC(2019)	1.96
NGC 4258	LTG	7.6	SABb	b	yes	no	yes	7.60 ± 0.01	DGC(2019)	2.12
NGC 4303	LTG	12.3	SBbc	b	yes	no	yes	6.58 ± 0.17	DGC(2019)	1.98
NGC 4388	LTG	17.8	SBcd	b	yes	no	yes	6.90 ± 0.11	DGC(2019)	2.00
NGC 4395	LTG	4.8	SBm	b	yes	no	yes	7.54 ± 0.17	DGC(2019)	1.42
NGC 4501	LTG	11.2	Sb	nb	yes	no	yes	7.13 ± 0.08	DGC(2019)	2.22
NGC 4594	LTG	9.6	Sa	nb	yes	no	yes	8.81 ± 0.03	DGC(2019)	2.35
NGC 4699	LTG	23.7	SABb	b	yes	no	no	8.34 ± 0.10	DGC(2019)	2.28
NGC 4736	LTG	4.4	SABab	nb	yes	no	yes	6.78 ± 0.10	DGC(2019)	2.03
NGC 4826	LTG	5.6	Sab	nb	yes	no	yes	6.07 ± 0.15	DGC(2019)	1.99
NGC 4945	LTG	3.7	SABc	nb	yes	no	yes	6.15 ± 0.30	DGC(2019)	2.07
NGC 5055	LTG	8.9	Sbc	nb	yes	no	no	8.94 ± 0.10	DGC(2019)	2.00
NGC 5495	LTG	101.1	SBc	b	yes	no	no	7.04 ± 0.08	DGC(2019)	2.22 [11g]
NGC 5765b	LTG	133.9	SABb	b	yes	no	no	7.72 ± 0.05	DGC(2019)	2.21 [11g]
NGC 6264	LTG	153.9	SBb	b	yes	no	yes	7.51 ± 0.06	DGC(2019)	2.20 [11f]
NGC 6323	LTG	116.9	SBab	b	yes	no	no	7.02 ± 0.14	DGC(2019)	2.20 [11f]
NGC 6926	LTG	86.6	SBc	b	yes	no	yes	7.74 ± 0.50	DGC(2019)	–
NGC 7582	LTG	19.9	SBab	b	yes	no	yes	7.67 ± 0.09	DGC(2019)	2.07
UGC 3789	LTG	49.6	SABa	b	yes	no	no	7.06 ± 0.05	DGC(2019)	2.03 [11f]
UGC 6093	LTG	152.8	SBbc	b	yes	no	no	7.41 ± 0.03	DGC(2019)	2.19 [11f]
NGC 0613	LTG	17.2	SB(rs)bc	b	yes	no	no	7.57 ± 0.15	Co+14(2019)	2.09
NGC 1365	LTG	17.8	SB(s)b	b	yes	no	yes	6.60 ± 0.30	Co+14(2019)	2.15
NGC 1566	LTG	7.2	SAB(s)bc	b	yes	no	yes	6.83 ± 0.30	Co+14(2019)	1.99
NGC 1672	LTG	11.4	SB(s)b	b	yes	no	yes	7.70 ± 0.10	Co+14(2019)	2.04
NGC 3504	LTG	13.6	SABab	b	yes	no	yes	7.01 ± 0.07	Ngu+10(2019)	2.08

NOTE—Column: (1) Galaxy name. (2) Galaxy type: early-type or late-type. (3) Distance of the galaxy. (4) Galaxy Morphology. (5) Presence of bar: b = barred, nb = non-barred. (6) Presence of a rotating intermediate-scale (ES) or large-scale (S0) disk. (7) Presence of a depleted core. (8) Presence of active galactic nucleus. (9) Directly measured black hole mass. (10) Catalog references, where the information for column (2) to column (9) comes from. SG(2016)= Savorgnan et al. (2016), GCS(2016)= Graham et al. (2016a), G+7(2016)= Graham et al. (2016b), SGD(2019)= Sahu et al. (2019), No+7(2007)= (Nowak et al. 2007), Ngu+10(2018)= Nguyen et al. (2018), Th+6(2019)= Thater et al. (2019), Bo+7(2019)= Boizelle et al. (2019), DGC(2019)= Davis et al. (2019), Co+14(2019)= Combes et al. (2019), Ngu+10(2019)= Nguyen et al. (2019). (11) Central velocity dispersion of galaxies mostly archived in HYPERLEDA (Paturel et al. 2003) unless otherwise specified. [11a]= Walsh et al. (2015), [11b]= Graham et al. (2016b), [11c]= Dalla Bontà et al. (2009), [11d]=Greene et al. (2010), [11e]=Thater et al. (2019), [11f]=Kormendy & Ho (2013), [11g]= Greene et al. (2016), [11h]= van den Bosch (2016), [11i]= Saglia et al. (2016). Bulge and galaxy stellar masses can also be found in Savorgnan & Graham (2016), Davis et al. (2019), and Sahu et al. (2019).

^a Latest black hole mass measurement from the Event Horizon Telescope Collaboration through direct imaging (Event Horizon Telescope Collaboration et al. 2019).

2.1. Galaxy Exclusions

We identify and exclude 13 galaxies which may bias the M – σ relation either because they are mergers, no-

table outliers, or at the end of the relation and thus able to torque the fit and thereby hinder efforts to detect departures from a single power-law. We are excluding galaxies: NGC 1316, NGC 5128, NGC 4342, NGC 4486B, NGC 404, NGC 5102, NGC 5206, NGC 7457, NGC 4395, NGC 5055, NGC 6926, NGC 4151, and NGC 3079, where the last five are LTGs.

We exclude NGC 1316, NGC 5128, NGC 4342, NGC 4486B, and NGC 404 following the galaxy exclusions in [Sahu et al. \(2019\)](#). This is also done in order to maintain consistency with the black hole mass versus spheroid and galaxy stellar mass relations, even though some of these galaxies do not seem to be significant outliers in our $M_{BH}-\sigma$ scaling relations. NGC 1316 and NGC 5128 are mergers in progress, which may have significant effects on their measured velocity dispersions. NGC 4342 ([Blom et al. 2014](#)) and NGC 4486B ([Batcheldor et al. 2010](#)) are heavily tidally stripped of their stellar mass by the gravitational pull of their massive companion galaxies NGC 4365 and NGC 4486 (M87), respectively. While NGC 404 is the only galaxy anchoring the intermediate black hole mass end ($\lesssim 10^5 M_\odot$) of the relation, it may potentially bias the best-fit line. Additionally, as we will see, NGC 404, NGC 5102, and NGC 5206, for whom we obtained black hole masses from the same group ([Nguyen et al. 2017, 2018](#)), seem to lie above the $M_{BH}-\sigma$ relation. They may not be outliers, but as we have only a few galaxies in the mass range $M_{BH} \lesssim 10^6 M_\odot$, we do not include them in our primary regressions. As noted above, this also serves to help us detect possible departures at the low-mass end.

NGC 7457, NGC 4395, and NGC 5055 have unusually low-velocity dispersion values, which makes them stand out from the, soon to be seen, best-fit lines. For NGC 6926, we do not have a reliable measurement of the velocity dispersion. Additionally, we exclude the LTGs NGC 4151 and NGC 3079 as they exert a disproportionate torque on the best-fit $M_{BH}-\sigma$ relations. Overall, we exclude a total of 13 galaxies, which leaves us with a reduced data-set of 130 galaxies.

3. $M_{BH}-\sigma$ RELATIONS

In this work we use both the BCES³ ([Akritas & Bershady 1996](#)) routine and the bisector line from the modified FITEXY routine (MPFITEXY, [Tremaine et al. 2002](#); [Novak et al. 2006](#); [Bedregal et al. 2006](#); [Williams et al. 2010](#); [Markwardt 2012](#)) to estab-

lish the $M-\sigma$ relations. Both the BCES and MPFITEXY regression routines take into account the measurement errors in the X and Y coordinates and allow for intrinsic scatter in the data.

The BCES routine directly provides the BCES(Y|X) line, the BCES(X|Y) line, and the regression line which symmetrically bisects the two, i.e., BCES(BISECTOR)⁴. However, to obtain a symmetrical treatment (MPFITEXY(BISECTOR)) of the data with the MPFITEXY routine requires averaging the slopes of the best-fit lines obtained from the forward (MPFITEXY(Y|X)) and inverse (MPFITEXY(X|Y)) regressions as explained in [Novak et al. \(2006\)](#).

We prefer the symmetric (bisector) regressions obtained from both the routines because we do not know whether the central SMBH mass fundamentally governs the central velocity dispersion of a galaxy or vice-versa. A symmetrical regression is also preferable for theoretical grounds, see [Novak et al. \(2006\)](#).

In our plots, we show the BCES(BISECTOR) regression line only, however asymmetric BCES(Y|X) and BCES(X|Y) regression parameters are also provided in [Table 2](#). We do not provide MPFITEXY best-fit parameters for our relations as these are consistent with the best-fit relations obtained from the BCES(Y|X) routine within the $\pm 1\sigma$ confidence limits.

Dividing our reduced sample of 130 galaxies into various categories, for example, early-type and late-type galaxies, Sérsic and core-Sérsic galaxies, galaxies with and without a disk, galaxies with and without a bar, and galaxies with and without an AGN, led us to some interesting $M_{BH}-\sigma$ relations. The following subsections describe the scaling relations obtained for these sub-morphological classes.

3.1. *Early-type Galaxies and Late-type Galaxies*

After excluding the galaxies mentioned in [Section ??](#), our reduced sample is comprised of 86 ETGs and 44 LTGs. The BCES(BISECTOR) regression line for the ETGs can be expressed as,

$$\log(M_{BH}/M_\odot) = (5.89 \pm 0.33) \log\left(\frac{\sigma}{200 \text{ km s}^{-1}}\right) + (8.30 \pm 0.05), \quad (1)$$

with a total rms scatter of $\Delta_{rms|BH} = 0.43$ dex in the $\log M_{BH}$ -direction. The relation followed by the LTGs

³ The BCES routine was used via the PYTHON module written by Rodrigo Nemmen ([Nemmen et al. 2012](#)), which is available at <https://github.com/rsnemmen/BCES>.

⁴ BCES(Y|X) minimizes the offsets in the Y-direction, and BCES(X|Y) minimizes, the offsets in the X-direction.

can be formulated as,

$$\log(M_{BH}/M_{\odot}) = (6.19 \pm 0.65) \log\left(\frac{\sigma}{200 \text{ km s}^{-1}}\right) + (8.22 \pm 0.12), \quad (2)$$

with $\Delta_{rms|BH} = 0.58$ dex. The slopes and intercepts of both lines (see Figure 1) are consistent within the $\pm 1\sigma$ confidence limits, suggesting a single $\log(M_{BH})$ versus σ relation for both ETGs and LTGs is adequate. Therefore, we perform a single regression on the total sample of 130 galaxies, which is represented in Figure 2. The BCES(BISECTOR) best-fit line obtained from the single regression can be written as

$$\log(M_{BH}/M_{\odot}) = (6.19 \pm 0.27) \log\left(\frac{\sigma}{200 \text{ km s}^{-1}}\right) + (8.26 \pm 0.04), \quad (3)$$

with $\Delta_{rms|BH} = 0.50$ dex. However, we will see in the following subsection, this is deceptive to think that one line is sufficient to understand the connection between super-massive black holes and the stellar velocity dispersion of the host galaxies.

Although we prefer to use a 10% uncertainty in the measured velocity dispersions for our galaxies, as discussed in Section 2, we find consistent results for our regressions when using the uncertainties provided in HYPERLEDA and the other corresponding sources (Column 11 of Table 1). In addition to the BCES(BISECTOR) regression line parameters, the slopes and intercepts of the best-fit lines from the BCES($M_{BH}|\sigma$) and BCES($\sigma|M_{BH}$) regressions, along with the scatter, Pearson correlation coefficient, and Spearman rank-order correlation coefficients are presented in Table 2.

In Figure 2, we show the galaxies NGC 404, NGC 5102, and NGC 5206 which are excluded from our regressions as these are the only data points in the low-mass ($M_{BH} \lesssim 10^6 M_{\odot}$) range. Taken from Nguyen et al. (2017, 2018), these may depart from the line for $M_{BH} \gtrsim 10^6 M_{\odot}$, perhaps revealing here a bend in the $M_{BH}-\sigma$ relation not detected by Nguyen et al. (2017, 2018). Including these galaxies in the regression produces a shallower slope of 5.72 ± 0.29 (cf. 6.19 ± 0.27 from Equation 3), suggesting these three galaxies may have a significant effect on our best-fit line for the full sample, which why is we decided to exclude them from our regressions. However, this shallower slope is still consistent (within $\pm 1\sigma$) with our current best-fit line (Equation 3).

In a recent work, van den Bosch (2016) fit a single line to all the morphological types of galaxies, and reported $M_{BH} \propto \sigma^{5.35 \pm 0.23}$, which is shallower than our relation (Equation 3). We suspect that their best-fit

line may be influenced by the inclusion of a few dwarf low-mass galaxies, the use of upper limits on M_{BH} for many galaxies, and 24 reverberation-mapped black hole mass estimates (pre-calibrated to a prior $M_{BH}-\sigma$ relation with a slope of 5.31 ± 0.33 from Woo et al. 2013).

3.2. Sérsic and Core-Sérsic Galaxies

Out of the 86 ETGs in our reduced sample, 34 are core-Sérsic, i.e., galaxies which have a deficit of stars at their center relative to the outer Sérsic profile (Graham et al. 2003), while the remaining 52 ETGs, and all 44 LTGs are Sérsic galaxies. Core-Sérsic or Sérsic classifications for each of our galaxies are borrowed from their parent works, i.e., Savorgnan et al. (2016), Davis et al. (2019), and Sahu et al. (2019) etc., as mentioned in Table 1 (Column 10).

We first performed separate regressions for the Sérsic and core-Sérsic ETGs, then on the combined sample of 130 galaxies. The $M_{BH}-\sigma$ plots for the two cases are shown in Figure 3 and Figure 4, respectively.

Sérsic and core-Sérsic categorization reveals two different relations followed by the two sub-populations. The symmetric best-fit line followed by the early-type Sérsic galaxies can be expressed as

$$\log(M_{BH}/M_{\odot}) = (5.14 \pm 0.37) \log\left(\frac{\sigma}{200 \text{ km s}^{-1}}\right) + (8.26 \pm 0.06), \quad (4)$$

with $\Delta_{rms|BH} = 0.41$ dex, represented by the dark blue line in Figure 3. The total Sérsic population, consisting of 96 early- and late-type Sérsic galaxies, produces the relation

$$\log(M_{BH}/M_{\odot}) = (5.86 \pm 0.33) \log\left(\frac{\sigma}{200 \text{ km s}^{-1}}\right) + (8.23 \pm 0.05), \quad (5)$$

represented by the dark blue line in Figure 4, with $\Delta_{rms|BH} = 0.51$ dex. The best-fit lines obtained for only early-type Sérsic galaxies and for all the Sérsic galaxies are marginally consistent with each other within the $\sim \pm 1\sigma$ bound of their slopes and intercepts.

However, the core-Sérsic galaxies follow a much steeper $M_{BH}-\sigma$ relation, with $\Delta_{rms|BH} = 0.47$ dex, as is shown by the dark red lines in both Figures 3 and 4, which can be expressed as

$$\log(M_{BH}/M_{\odot}) = (8.54 \pm 1.07) \log\left(\frac{\sigma}{200 \text{ km s}^{-1}}\right) + (7.93 \pm 0.20). \quad (6)$$

The slope of this line is inconsistent with that of the Sérsic galaxies. The difference in their slopes emphasizes that Sérsic and core-Sérsic galaxies follow two distinct relations, potentially linked to the evolutionary paths

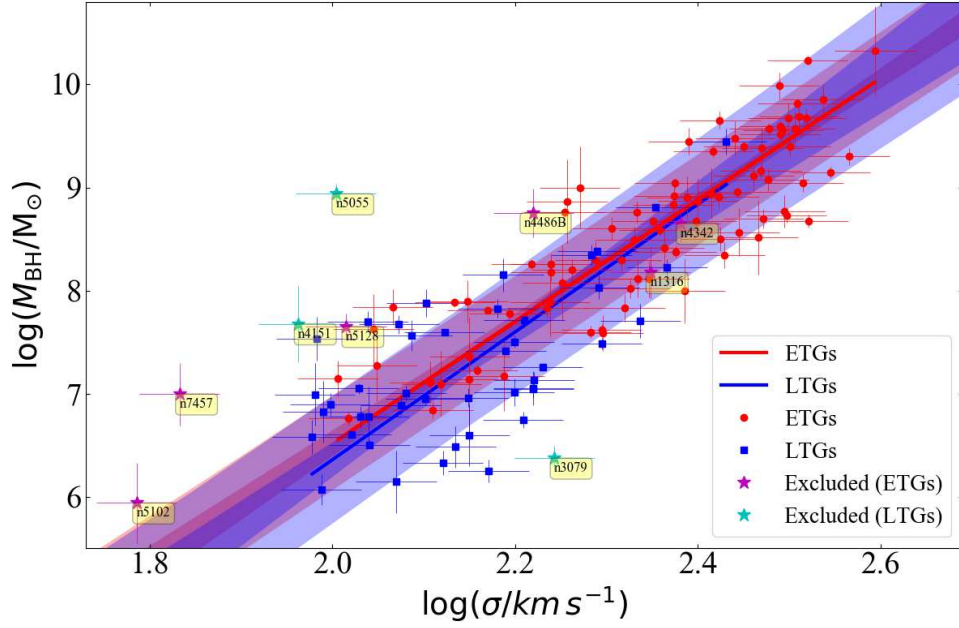


Figure 1. Black hole mass versus central velocity dispersion relation followed by ETGs (red circles) and LTGs (blue squares). Dark red and blue lines are the BCES(BISECTOR) best-fit lines for ETGs and LTGs. The red and blue bands around these lines represent the $\pm 1\sigma$ uncertainty limits in their slopes and the intercepts. Furthermore, the light red and light blue shaded regions depict the $\pm 1\sigma$ scatter in the ETG and LTG samples, respectively. The best-fit lines for the two sub-populations are almost overlapping and consistent (Equations 1 and 2) with each other, suggesting a single $M_{BH}-\sigma$ relation as is shown in Figure 2.

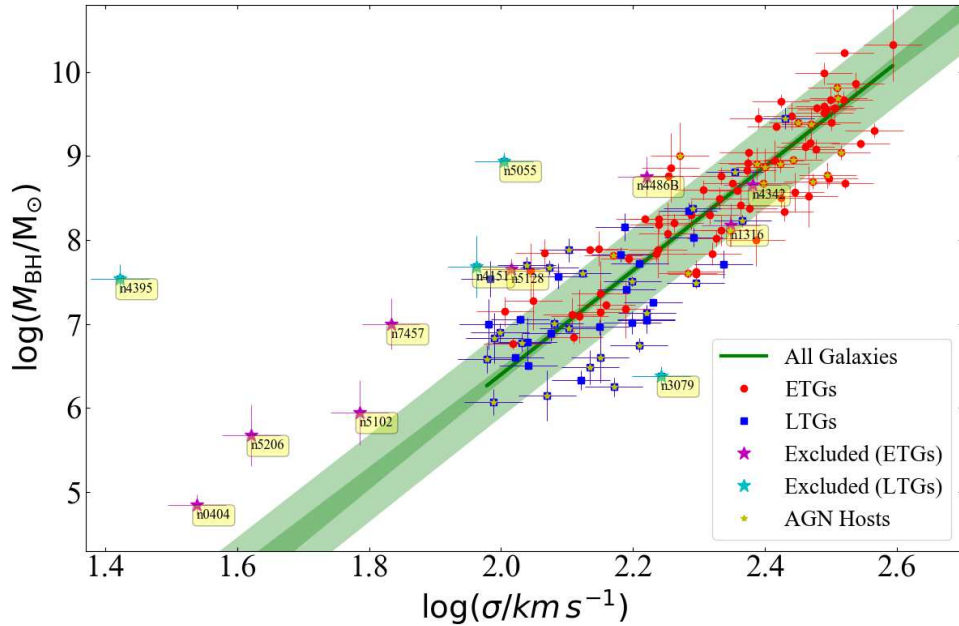


Figure 2. Black hole mass versus central velocity dispersion relation obtained from a single regression on the sample including 130 ETGs and LTGs. The dark green line is the best-fit BCES(BISECTOR) regression line for the whole sample (Equation 3). The dark green band around the dark green line shows the $\pm 1\sigma$ uncertainty in the slope and intercept of the best-fit line. The light green shaded region represents the $\pm 1\sigma$ scatter in the data. This explanation of the dark and light shaded regions around the best-fit line applies to all the subsequent figures in this paper.

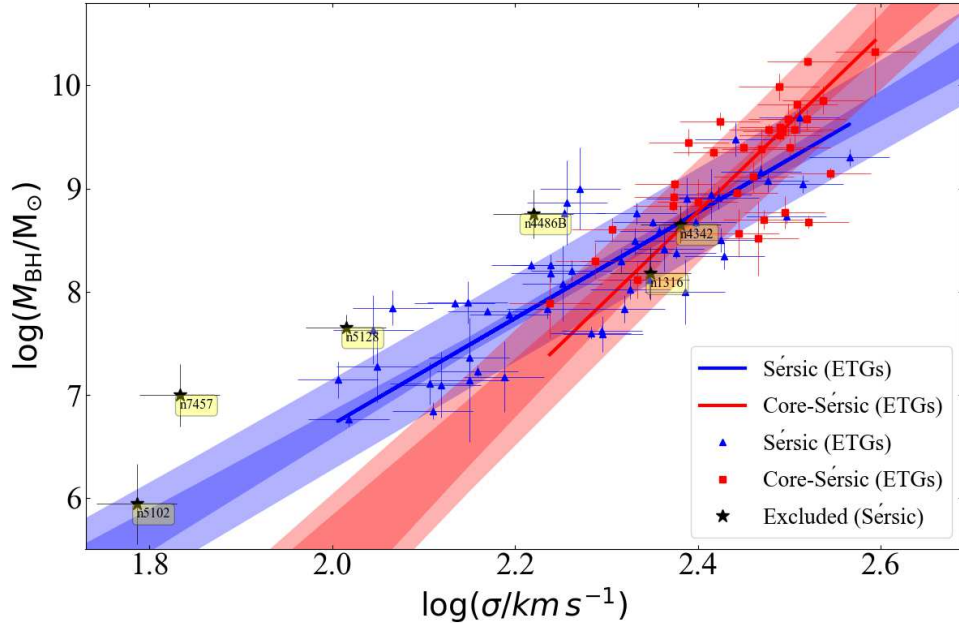


Figure 3. Black hole mass versus central velocity dispersion relation for Sérsic (blue triangles) and core-Sérsic (red squares) ETGs. These two sub-populations follow two distinct relations (Equations 4 and 6), suggesting a bend in the $M_{BH}-\sigma$ relation.

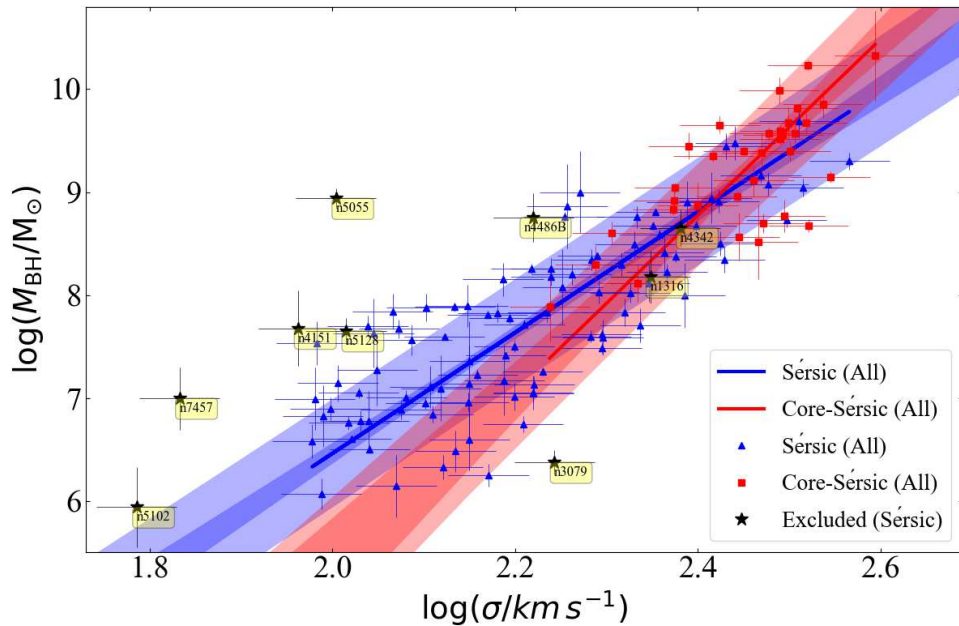


Figure 4. Similar to Figure 3, but including all early- and late-type Sérsic galaxies in the same the category (blue triangles) while all core-Sérsic galaxies (red squares) are early-type only. On including LTGs (spirals) which are all Sérsic galaxies, we still find the bend in the $M_{BH}-\sigma$ relation, such that all Sérsic and core-Sérsic galaxies follow two different relations (Equations 5 and 6).

followed by these two types of galaxies, i.e., evolution via dry-mergers versus gas-rich mergers. Additionally, although core-Sérsic galaxies follow a steeper relation, their σ values do not appear to saturate or asymptote at the high black hole mass end.

Core-Sérsic galaxies are old, gas-poor, massive galaxies, many of which are BCGs which have undergone multiple major (equal mass) dissipation-less dry-mergers. During a dry-merger, their central SMBHs inspiral, expelling out stars from the center, thereby creating a deficit of light at the core of the resulting galaxy. The extent of the deficit is potentially a measure of the number of dry mergers the galaxy has undergone (Merritt & Milosavljević 2005; Savorgnan & Graham 2015). The size of the core also appears to grow in proportion to the black hole mass (Dullo & Graham 2014; Thomas et al. 2016; Mehrگان et al. 2019).

The steeper slope found here for core-Sérsic galaxies suggests that these massive galaxies, while evolving through mergers, increase their black hole masses, spheroid and total galaxy masses, but their velocity dispersion does not keep the same pace. This has also been suggested by some theoretical studies (e.g., Ciotti & van Albada 2001; Oser et al. 2012; Shankar et al. 2013; Hilz et al. 2013). Furthermore, Volonteri & Ciotti (2013) used their analytical and semi-analytical models to show that BCGs are found to be offset in the $M_{BH}-\sigma$ relation because they undergo multiple gas-poor (dry) mergers resulting in over-massive black holes with only mildly increased velocity dispersion. These scenarios can be compared with the recent analytical arguments from King & Nealon (2019), which shows that for the ultra-massive black holes, late-epoch interactions can reduce their velocity dispersions and leave them above the $M_{BH}-\sigma$ relation.

Sérsic galaxies evolve through either wet (gas-rich) mergers or accretion of gas from their surroundings. The $M_{BH}-\sigma$ relation obtained for Sérsic galaxies suggests that while evolving, their stellar velocity dispersions also increase significantly along with the increase in their black hole masses and total galaxy masses.

3.3. Galaxies With a Disk (ES/S0/Sp) and Without a Disk (E)

Elliptical (E) galaxies are pressure supported, spheroid-dominated galaxies with minimal rotation. Lenticular (ES), lenticular (S0), and spiral (Sp) galaxies have a rotating disk which is either large-scale and extends out of the bulge in the latter two types (S0 and Sp), or of intermediate-scale in the ES galaxies (Liller 1966; Graham et al. 2016a; Graham 2019). Our reduced

sample is comprised of 43 elliptical galaxies which do not have a rotating disk, plus 87 galaxies with a disk, which includes 43 ES or S0-types (ETGs) and 44 spirals (LTGs).

We first performed separate regressions on the ETGs with (ES/S0) and without (E) a disk, as shown in Figure 5. Then we performed regressions on all types of galaxies with a disk (ES/S0/Sp), and without a disk (E-types), as represented in Figure 6. Interestingly, we again find a bend in the $M_{BH}-\sigma$ relation in both the plots, similar to the bend due to Sérsic and core-Sérsic galaxies, but less pronounced. The relation followed by the 43 elliptical galaxies, which do not have any intermediate- or large-scale disk, is

$$\log(M_{BH}/M_{\odot}) = (6.96 \pm 0.62) \log\left(\frac{\sigma}{200 \text{ km s}^{-1}}\right) + (8.19 \pm 0.10), \quad (7)$$

with $\Delta_{rms|BH} = 0.42$ dex. The 43 ETGs (ES and S0-types), which have either an intermediate- or large-scale rotating disk, follow the relation

$$\log(M_{BH}/M_{\odot}) = (5.15 \pm 0.39) \log\left(\frac{\sigma}{200 \text{ km s}^{-1}}\right) + (8.27 \pm 0.06), \quad (8)$$

with $\Delta_{rms|BH} = 0.43$ dex.

Upon including spiral galaxies (LTGs), all of which have a large-scale disk, the slope of the best-fit line defined by galaxies with a disk increases to become

$$\log(M_{BH}/M_{\odot}) = (5.88 \pm 0.34) \log\left(\frac{\sigma}{200 \text{ km s}^{-1}}\right) + (8.23 \pm 0.06), \quad (9)$$

with $\Delta_{rms|BH} = 0.52$ dex. The apparent bend in the $M_{BH}-\sigma$ relation is reduced (Figure 6), with the slope of the line followed by galaxies with a disk mildly inconsistent with that of the line followed by the elliptical disk-less galaxies.

This slight bend in the $M_{BH}-\sigma$ relation due to galaxies with and without a disk is likely because most of the elliptical galaxies in our sample are massive core-Sérsic galaxies and almost all the galaxies with a rotating disk are Sérsic galaxies. The extent of the bend found in the $M_{BH}-\sigma$ relation due to core-Sérsic and Sérsic galaxies is greater than the bend in the relations followed by the galaxies with and without a disk. This suggests that the bend in the $M_{BH}-\sigma$ relation is predominantly caused by core-Sérsic versus Sérsic galaxies. It should be noted that core-Sérsic galaxies can also have disks (e.g. Dullo & Graham 2013, 2014; Dullo 2014).

We speculate that Savorgnan & Graham (2015) failed to detect a significant bend in the $M_{BH}-\sigma$ relation due

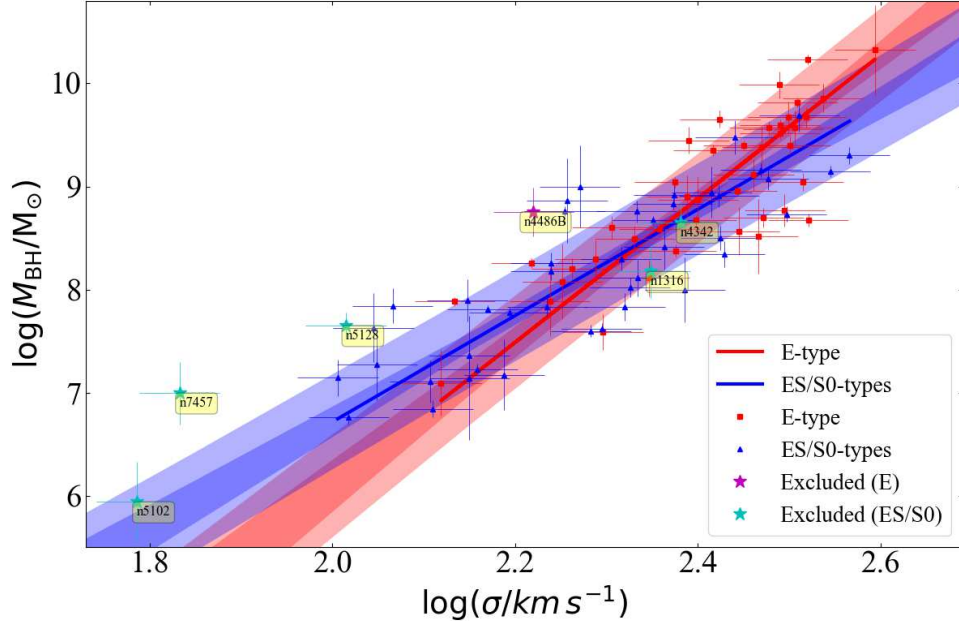


Figure 5. Black hole mass versus central velocity dispersion relations for ETGs with a disk (ES/S0-types, Equation 8) and ETGs without a disk (E-type, Equation 7). We recover the bend in the $M_{BH}-\sigma$ relation found in Section 3.2 due to Sérsic and core-Sérsic galaxies (see Figure 3), as most of the elliptical galaxies in our sample are core-Sérsic galaxies and most of the ETGs with a disk (ES/S0-types) are Sérsic galaxies.

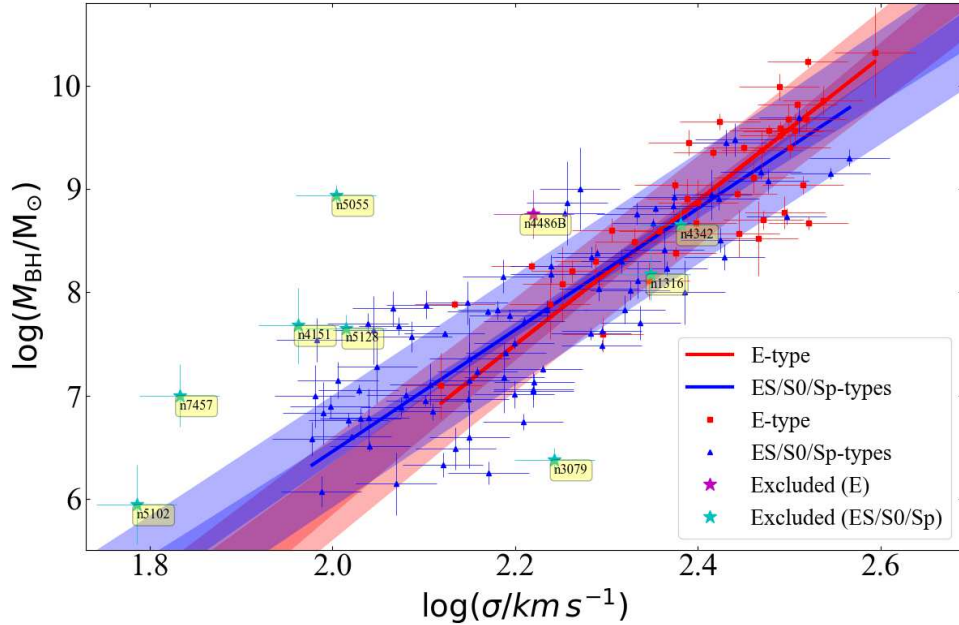


Figure 6. Similar to Figure 5, but now including spiral (Sp) galaxies, all of which have an extended rotating disk, along with early-type elliptical (ES) and lenticular (S0) galaxies in the category of galaxies with a disk (Equation 9), while elliptical (E) galaxies without a disk are all ETGs (Equation 7). We again find a bend in the $M_{BH}-\sigma$ relation, but not as pronounced as between Sérsic and core-Sérsic galaxies (Figure 4).

to core-Sérsic and Sérsic galaxies, or slow and fast rotators⁵, because of their smaller sample size. However, some of their galaxies can be spotted to be offset from their $M_{BH}-\sigma$ relation at the high-mass end.

3.4. Barred and Non-barred Galaxies

In the past, some observational works (Graham 2007; Hu 2008; Graham 2008a,b) and simulations (Brown et al. 2013; Hartmann et al. 2014) have revealed that barred galaxies are offset towards the higher σ side in the $M_{BH}-\sigma$ diagram. Based on that offset, these studies suggest that barred galaxies should be separated from non-barred galaxies in order to obtain $M_{BH}-\sigma$ relations for barred and non-barred galaxies.

To investigate the above offset using our larger dataset, accompanied with our revised classification based upon multi-component decompositions, we also divided our sample into barred and non-barred galaxies, and performed separate regressions on both populations. This was first done for barred and non-barred ETGs, then using the total (reduced) sample, as shown in Figures 7 and 8, respectively. Our ETG sample consists of 16 barred and 70 non-barred galaxies, while the full sample comprises 47 barred and 83 non-barred galaxies.

Surprisingly, we do not find any offset between barred and non-barred galaxies, in both cases, i.e., only ETGs and the ETG + LTG sample. The best-fit line for the 16 barred ETGs is

$$\log(M_{BH}/M_{\odot}) = (6.15 \pm 0.90) \log\left(\frac{\sigma}{200 \text{ km s}^{-1}}\right) + (8.23 \pm 0.16), \quad (10)$$

with $\Delta_{rms|BH} = 0.42$ dex. However, we require a larger sample of barred ETGs for a robust relation. The 70 non-barred ETGs define the following relation, with $\Delta_{rms|BH} = 0.42$,

$$\log(M_{BH}/M_{\odot}) = (5.63 \pm 0.42) \log\left(\frac{\sigma}{200 \text{ km s}^{-1}}\right) + (8.34 \pm 0.06). \quad (11)$$

The 47 barred ETG + LTG population defines the line,

$$\log(M_{BH}/M_{\odot}) = (5.57 \pm 0.54) \log\left(\frac{\sigma}{200 \text{ km s}^{-1}}\right) + (8.19 \pm 0.10), \quad (12)$$

with $\Delta_{rms|BH} = 0.48$ dex. The 83 non-barred galaxies define the relation

$$\log(M_{BH}/M_{\odot}) = (6.34 \pm 0.43) \log\left(\frac{\sigma}{200 \text{ km s}^{-1}}\right) + (8.25 \pm 0.06), \quad (13)$$

with $\Delta_{rms|BH} = 0.50$ dex. The best-fit lines for the barred and non-barred galaxies are consistent within the $\pm 1\sigma$ bounds of their slopes and intercepts, suggesting no significant offset between barred and non-barred galaxies.

3.4.1. Investigating Previous Offsets

In order to find the reason behind the offset observed in Graham & Scott (2013), we have compared their regression lines with ours obtained using the latest M_{BH} , σ data, and updated bar-morphologies. Their sample of 72 galaxies was comprised of 21 barred and 51 non-barred galaxies, according to the morphological classifications they adopted, which were obtained from the NASA/IPAC Extragalactic Database (NED). All of their galaxies are present in our current sample, and in order to make a comparison, we use only the galaxies present in the data-set of Graham & Scott (2013).

Interestingly, in our reduced sample of 130 galaxies, out of those common 72 galaxies, we have classified 27 as barred, and 45 as non-barred. The barred and non-barred classifications for our current sample are based on the morphologies obtained from the multi-component decompositions of these galaxies presented in our recent works (Savorgnan & Graham 2016; Davis et al. 2019; Sahu et al. 2019). We notice that in the data-set of Graham & Scott (2013), seven barred galaxies (NGC 224, NGC 2974, NGC 3245, NGC 3998, NGC 4026, NGC 4388, and NGC 6264) were misclassified as non-barred, possibly due to the weak presence of bars. Also, one non-barred galaxy (NGC 4945) in their sample appears to have been misclassified as barred, with (Davis et al. 2019) reporting only a nuclear bar too weak to include in their modelling.

We also noticed that the latest updated velocity dispersion for of the barred spiral galaxy NGC 4151 is 91.8 km s^{-1} , which is notably different from the old reported value of 156 km s^{-1} by HYPERLEDA. The considerable difference now makes this galaxy stand out in the $M_{BH}-\sigma$ diagram. Therefore, as noted in Section ??, we excluded this galaxy from our regressions. Thus, we used only 71 galaxies from our current sample for the comparison, which is represented in Figure 9.

The green and yellow lines in Figure 9 are the BCES symmetric best-fit lines from Graham & Scott (2013) for the barred and non-barred galaxies, respectively. These two lines are offset by ~ 0.5 dex at the median velocity dispersion of 200 km s^{-1} . The blue and red BCES bisector lines for the same barred and non-barred galaxies from our current data-set (minus NGC 4151), are offset by only 0.15 dex. Moreover, on using the total (reduced) sample of 130 galaxies comprising 47 barred and 83 non-

⁵ Note: ES galaxies are both fast rotators and slow rotators (e.g., Bellstedt et al. 2017).

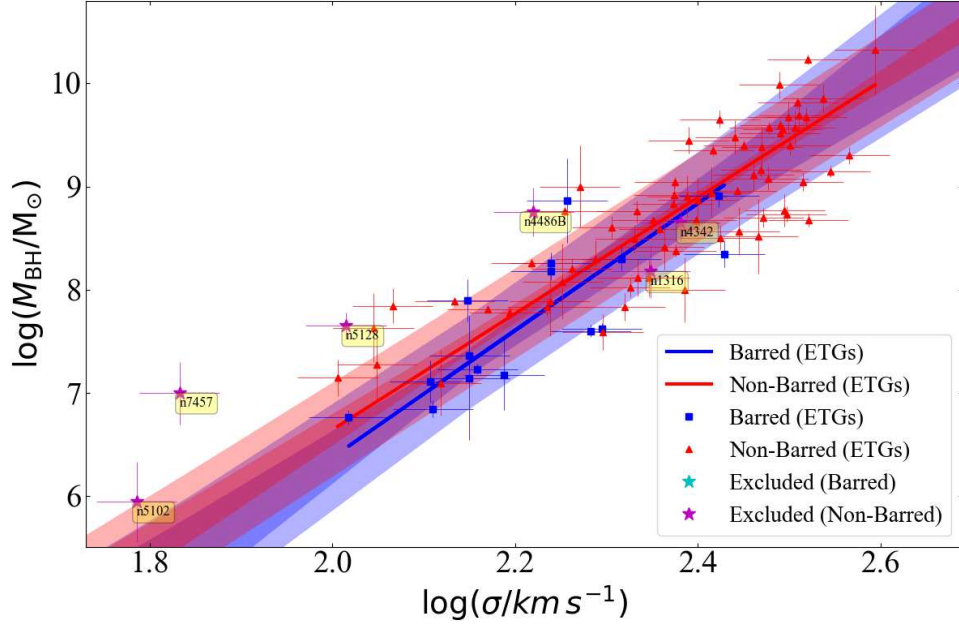


Figure 7. Black hole mass versus central velocity dispersion relation for barred and non-barred ETGs. Although we only have a small sample of 16 barred ETGs, the consistency of the two regression lines (blue and red lines) suggests no offset between barred (Equation 10) and non-barred (Equation 11) ETGs in the M_{BH} - σ diagram.

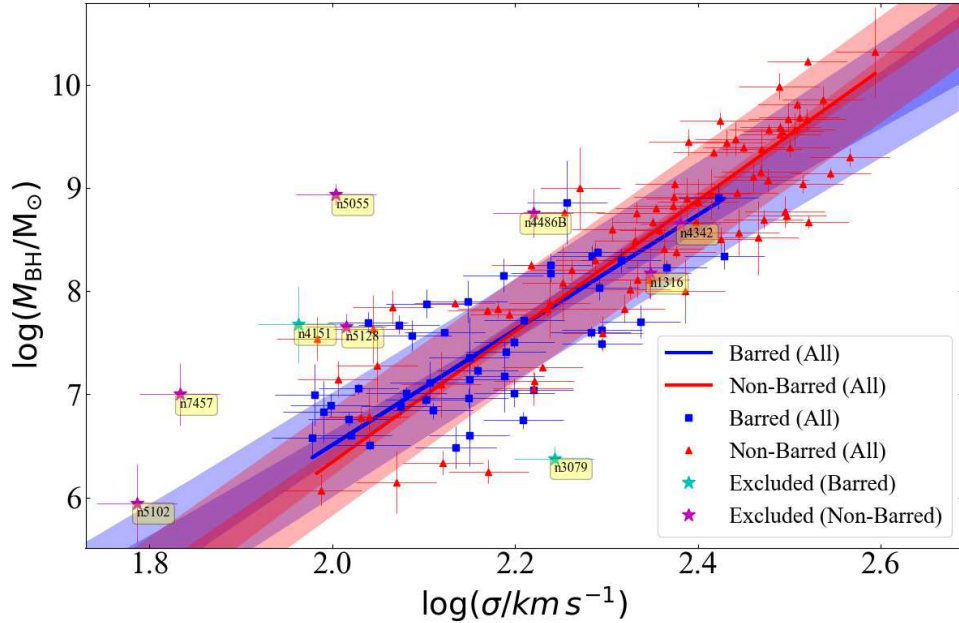


Figure 8. Similar to Figure 7, but including barred and non-barred late-type galaxies as well. The regression lines obtained for the 47 barred (blue line, Equation 12) and 83 non-barred (red line, Equation 13) galaxies are overlapping and consistent with each other, implying no-offset between barred and non-barred galaxies.

barred galaxies, as is represented in Figure 8, the offset reduces to less than 0.1 dex (see Equations 12 and 13).

We find that there are two main reasons why Graham & Scott (2013) found an offset. First, they largely classified their galaxies as barred or non-barred based on the morphologies provided by NED, which are mainly from the RC3 catalog (de Vaucouleurs et al. 1991) and in many cases it failed to identify bars and some other galaxy structures as well. The second reason is that their sample of 72 galaxies lacked (a sufficiently large sample of) barred galaxies above their regression line (the green line in Figure 9). Another reason for the difference might have been the updated black hole masses and velocity dispersions, but we have found that this does not seem to have a significant effect on the offset between the regression lines for the barred and non-barred galaxies.

3.4.2. Strong versus Weak or Faint Bars

We also investigated if weak/faint barred galaxies are biasing our $M_{BH}-\sigma$ relation (Equation 12) for all the barred galaxies. There was a possibility that perhaps most of the weak/faint barred galaxies fall above the best-fit (blue line in Figure 8) line for the barred galaxies in our current sample, and thereby reduce the offset between the best-fit line for barred and non-barred galaxies.

For this investigation, we used the bar-to-total (galaxy) luminosity (L_{bar}/L_{tot}) ratio to categorize our barred galaxies into strong and weak/faint categories. However, as we were not sure of where to make the cut, we performed this test twice, first making the division at $L_{bar}/L_{tot} = 0.05$, then at $L_{bar}/L_{tot} = 0.1$. Figure 10 shows the barred galaxies color coded as black strong-barred ($L_{bar}/L_{tot} \geq 0.1$), yellow faint-barred ($L_{bar}/L_{tot} \leq 0.05$), and green with intermediate bar strength ($0.05 < L_{bar}/L_{tot} < 0.1$). For 13 barred-galaxies, 8 of which are from (Savorgnan & Graham 2016), 4 are from Combes et al. (2019), and one is from Nguyen et al. (2019), we do not have bar-magnitudes. Hence, we categorized them on the basis of their multi-component decomposition profile, the morphological bar classification provided by the literature, and a visual inspection of their images which was also done for all the other barred galaxies. Overall, our total sample of 47 barred galaxies consists of 25 strong, 10 weak/faint, and 12 intermediate-strength barred galaxies.

For the first test, i.e., for the division at $L_{bar}/L_{tot} = 0.05$, all the strong (and intermediate) barred galaxies are distributed almost uniformly about the best-fit (blue) line for the barred galaxies, and many of the faint barred galaxies are below the best-fit line (see Fig-

ure 10). This suggests that galaxies with faint-bars do not minimize the offset between barred and non-barred galaxies. As for the second cut at $L_{bar}/L_{tot} = 0.1$, we can see in Figure 10, that most of the intermediate and faint barred galaxies are below the best-fit line for barred-galaxies, again indicating that weak/faint-barred, or even intermediate-barred galaxies in our sample do not take part in reducing the offset between barred and non-barred galaxies. Strongly-barred galaxies are distributed above and below the best-fit line for barred galaxies.

3.5. Galaxies with and without an AGN

Our reduced sample of 130 galaxies includes 39 galaxies hosting an AGN, which are pointed out in Figure 2. We identified the AGN hosts using the 13th edition of the catalog of quasars and active nuclei presented by Véron-Cetty & Véron (2010). Interestingly, these AGN hosts are spread almost uniformly about the best-fit bisector regression line (for the reduced sample of 130 galaxies) for the range of M_{BH} and σ that we have, indicating that galaxies with and without an AGN both follow a single relation.

Also, on performing separate regressions on AGN hosts and galaxies without AGN, we obtain almost overlapping regression lines for the two categories, such that their slopes and intercept are consistent with each other within the $\pm 1\sigma$ confidence bounds (Figure 11). The regression parameters for the best-fit lines for galaxies with and without AGNs are given in Table 2.

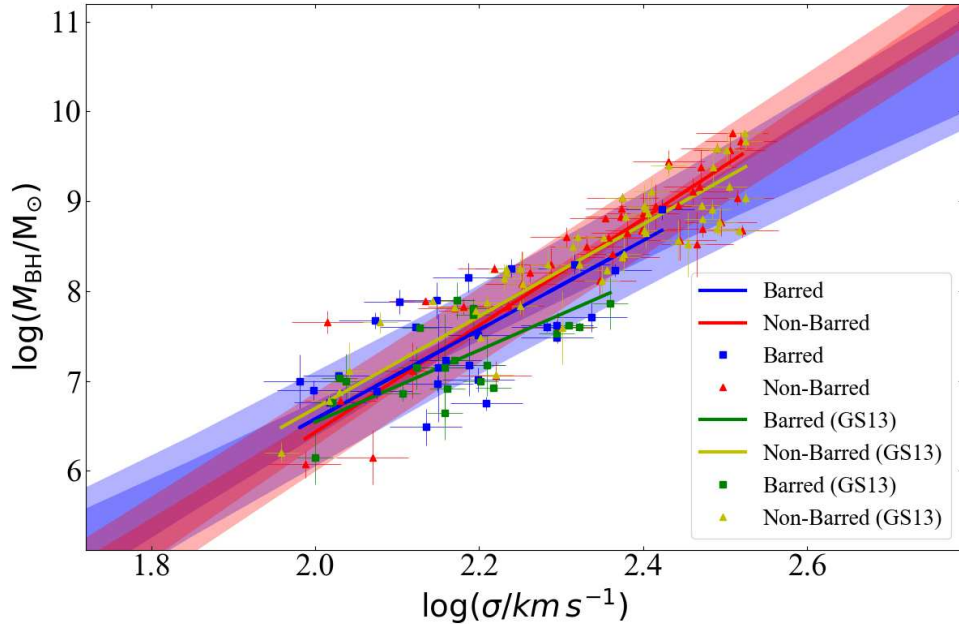


Figure 9. Comparison of our $M_{BH}-\sigma$ relations for barred and non-barred galaxies with the relations reported in [Graham & Scott \(2013, GS13\)](#). Their galaxy sample is a sub-set of our current sample, thus for a comparison, we use our latest data for the galaxies in their sample (minus NGC 4151), applied with our new bar morphologies (blue and red points). The barred and non-barred data points (i.e., the green squares and yellow triangles, respectively) of [Graham & Scott \(2013\)](#) represent the M_{BH} , σ , and bar classifications they used. Using the same galaxy sample as that of [Graham & Scott \(2013\)](#), we do not find any significant offset between barred and non-barred galaxies.

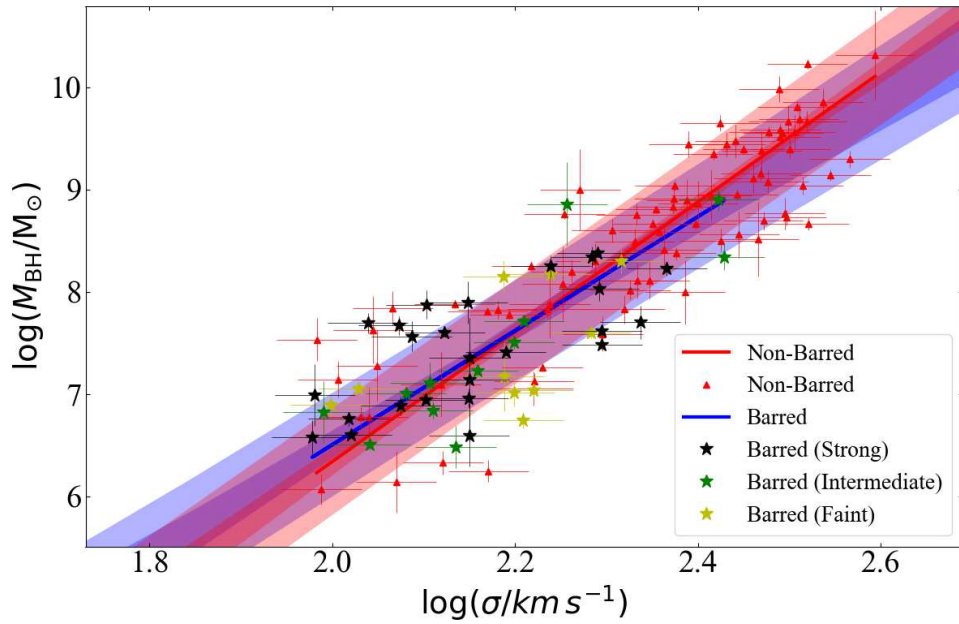


Figure 10. Similar to Figure 8, but now categorizing our barred galaxies into strong, intermediate, and faint barred galaxies.

Table 2. Linear Regressions [$\log(M_{BH}/M_{\odot}) = \alpha \log(\sigma/200) + \beta$]

Regression	Minimization	α	β	ϵ	$\Delta_{rms BH}$	r	r_s
(1)	(2)	(3)	(dex) (4)	(dex) (5)	(dex) (6)	(7)	(8)
Early-Type and Late-Type Galaxies							
86 Early-Type Galaxies							
BCES(<i>Bisector</i>)	<i>Symmetric</i>	5.89 ± 0.33	8.30 ± 0.05	0.30	0.43	} 0.87	0.86
BCES($M_{BH} \sigma$)	M_{BH}	5.45 ± 0.35	8.32 ± 0.05	0.30	0.42		
BCES(σM_{BH})	σ	6.41 ± 0.35	8.27 ± 0.06	0.32	0.46		
44 Late-Type Galaxies							
BCES(<i>Bisector</i>)	<i>Symmetric</i>	6.19 ± 0.65	8.22 ± 0.12	0.51	0.58	} 0.67	0.59
BCES($M_{BH} \sigma$)	M_{BH}	4.68 ± 0.79	7.99 ± 0.15	0.48	0.54		
BCES(σM_{BH})	σ	9.06 ± 1.20	8.67 ± 0.22	0.68	0.78		
Single regression on (130) Early and Late-Type Galaxies							
BCES(<i>Bisector</i>)	<i>Symmetric</i>	6.19 ± 0.27	8.26 ± 0.04	0.38	0.50	} 0.88	0.89
BCES($M_{BH} \sigma$)	M_{BH}	5.70 ± 0.28	8.25 ± 0.04	0.38	0.48		
BCES(σM_{BH})	σ	6.76 ± 0.29	8.27 ± 0.04	0.41	0.53		
Sérsic and Core-Sérsic Galaxies							
96 Sérsic Galaxies							
BCES(<i>Bisector</i>)	<i>Symmetric</i>	5.86 ± 0.33	8.23 ± 0.05	0.41	0.51	} 0.82	0.81
BCES($M_{BH} \sigma$)	M_{BH}	5.13 ± 0.33	8.17 ± 0.05	0.40	0.49		
BCES(σM_{BH})	σ	6.82 ± 0.45	8.31 ± 0.06	0.46	0.57		
34 Core-Sérsic Galaxies							
BCES(<i>Bisector</i>)	<i>Symmetric</i>	8.54 ± 1.07	7.93 ± 0.20	0.26	0.47	} 0.72	0.65
BCES($M_{BH} \sigma$)	M_{BH}	7.60 ± 1.10	8.07 ± 0.17	0.26	0.43		
BCES(σM_{BH})	σ	9.76 ± 1.74	7.75 ± 0.32	0.28	0.52		
Galaxies with and without a disk							
87 ES, S0, Sp-Type Galaxies							
BCES(<i>Bisector</i>)	<i>Symmetric</i>	5.88 ± 0.34	8.23 ± 0.06	0.43	0.52	} 0.82	0.80
BCES($M_{BH} \sigma$)	M_{BH}	5.13 ± 0.34	8.16 ± 0.06	0.42	0.50		
BCES(σM_{BH})	σ	6.87 ± 0.47	8.31 ± 0.07	0.48	0.59		
43 E-Type Galaxies							
BCES(<i>Bisector</i>)	<i>Symmetric</i>	6.96 ± 0.62	8.19 ± 0.10	0.27	0.42	} 0.84	0.82
BCES($M_{BH} \sigma$)	M_{BH}	6.43 ± 0.66	8.25 ± 0.09	0.26	0.40		
BCES(σM_{BH})	σ	7.58 ± 0.72	8.12 ± 0.13	0.28	0.45		
Galaxies with and without a bar							
47 Barred Galaxies							
BCES(<i>Bisector</i>)	<i>Symmetric</i>	5.57 ± 0.54	8.19 ± 0.10	0.38	0.48	} 0.72	0.69
BCES($M_{BH} \sigma$)	M_{BH}	4.52 ± 0.52	8.05 ± 0.10	0.37	0.44		
BCES(σM_{BH})	σ	7.25 ± 0.97	8.41 ± 0.16	0.47	0.58		
83 Non-Barred Galaxies							
BCES(<i>Bisector</i>)	<i>Symmetric</i>	6.34 ± 0.43	8.25 ± 0.06	0.38	0.50	} 0.87	0.87
BCES($M_{BH} \sigma$)	M_{BH}	5.80 ± 0.44	8.28 ± 0.06	0.38	0.48		
BCES(σM_{BH})	σ	7.00 ± 0.45	8.22 ± 0.07	0.41	0.54		
Galaxies with and without an AGN							

Table 2 *continued*

Table 2 (continued)

Regression	Minimization	α	β	ϵ	$\Delta_{rms BH}$	r	r_s
(1)	(2)	(3)	(4)	(5)	(6)	(7)	(8)
39 AGN host Galaxies							
BCES(<i>Bisector</i>)	<i>Symmetric</i>	6.36 ± 0.45	8.21 ± 0.08	0.46	0.55	0.87	0.84
BCES($M_{BH} \sigma$)	M_{BH}	5.69 ± 0.45	8.18 ± 0.08	0.45	0.53		
BCES(σM_{BH})	σ	7.22 ± 0.55	8.25 ± 0.09	0.51	0.61		
91 Galaxies without AGN							
BCES(<i>Bisector</i>)	<i>Symmetric</i>	6.04 ± 0.31	8.29 ± 0.05	0.35	0.47	0.88	0.89
BCES($M_{BH} \sigma$)	M_{BH}	5.59 ± 0.34	8.28 ± 0.05	0.35	0.46		
BCES(σM_{BH})	σ	6.57 ± 0.32	8.29 ± 0.05	0.37	0.50		

NOTE— Columns: (1) Type of regression performed. (2) The coordinate direction in which the offsets from the regression line is minimized. (3) Slope of the regression line. (4) Intercept of the regression line. (5) Intrinsic scatter in the $\log M_{BH}$ -direction (using Equation 1 from [Graham & Driver 2007](#)). (6) Total root mean square (rms) scatter in the M_{BH} direction. (7) Pearson correlation coefficient. (8) Spearman rank-order correlation coefficient.

A galaxy hosting an AGN can be Sérsic or core-Sérsic, as can a galaxy without an AGN; hence, regardless of whether a galaxy hosts an AGN or not, the M_{BH} - σ relations defined by Sérsic and core-Sérsic galaxies remain applicable, and should be used depending on the presence or absence of a core (deficit of star light, not due to dust obstruction).

4. INTERNAL CONSISTENCY BETWEEN THE M_{BH} - $M_{*,GAL}$, M_{BH} - $M_{*,SPH}$, AND M_{BH} - σ RELATIONS

Recent works by [Sahu et al. \(2019\)](#) and [Davis et al. \(2019\)](#) established robust M_{BH} - $M_{*,gal}$ and M_{BH} - $M_{*,sph}$ correlations for ETGs and LTGs, using a (reduced) sample of 76 ETGs and 40 LTGs, respectively. As elaborated above in Section 3, we also observe a strong correlation between black hole mass and the central stellar velocity dispersion, along with the discovery of a bend in the M_{BH} - σ relation due to Sérsic and core-Sérsic galaxies.

The M_{BH} - $M_{*,gal}$ (and M_{BH} - $M_{*,sph}$) relations combined with our bent M_{BH} - σ relations can predict the $M_{*,gal}$ - σ and $M_{*,sph}$ - σ relations. They should be compared with the observed $M_{*,gal}$ - σ and $M_{*,sph}$ - σ relations to check for internal consistency of our relations. The ETGs and LTGs of [Sahu et al. \(2019\)](#) and [Davis et al. \(2019\)](#), respectively, constitute $\approx 90\%$ of the sample used in this work to obtain the M_{BH} - σ relations, hence their M_{BH} - $M_{*,gal}$ and M_{BH} - $M_{*,sph}$ relations are appropriate for internal consistency checks.

Sérsic and core-Sérsic ETGs have been found to follow the same M_{BH} - $M_{*,gal}$ and M_{BH} - $M_{*,sph}$ relations in [Sahu et al. \(2019\)](#), such that $M_{BH} \propto M_{*,gal}^{1.65 \pm 0.11}$ and $M_{BH} \propto M_{*,sph}^{1.27 \pm 0.07}$ for all ETGs, i.e., when com-

paring those with a disk and those without a disk. Whereas, the LTGs in [Davis et al. \(2019\)](#), all of which are Sérsic, define the relations $M_{BH} \propto M_{*,gal}^{3.05 \pm 0.70}$ and $M_{BH} \propto M_{*,sph}^{2.16 \pm 0.32}$, with slopes almost twice that of the (single regression) slopes for ETGs in [Sahu et al. \(2019\)](#), see their Figure 11). However, separating the ETGs into those with and without a disk reveals that they follow two different M_{BH} - $M_{*,sph}$ relations with slopes of approximately 1.9 ± 0.2 but with intercepts offset by more than a factor of 10 in the M_{BH} -direction. In the M_{BH} - $M_{*,gal}$ diagram, the two relations for ETGs with and without a disk agree with each other much more closely, suggesting that the M_{BH} - $M_{*,gal}$ relation obtained from the single regression is a reasonable approximation for ETGs with and without a disk. In the M_{BH} - σ diagram, Sérsic and core-Sérsic galaxies in our total (ETG+LTG) sample define two distinct relations, see Equations 5 and 6, respectively.

Theoretically, to check the consistency between the M_{BH} - $M_{*,sph}$, M_{BH} - σ , and $M_{*,sph}$ - σ relations for ETGs, we should use the two different relations for ETGs with and without disk on the M_{BH} - $M_{*,sph}$ diagram (as mentioned above) with the two M_{BH} - σ relations for core-Sérsic and Sérsic ETGs (Section 3.2), to predict different $M_{*,sph}$ - σ relations for core-Sérsic ETGs with and without a disk and Sérsic ETGs with and without a disk. However, if we separate the core-Sérsic (or Sérsic) ETGs into galaxies with and without a disk, each sub-population will be too small to derive a robust $M_{*,sph}$ - σ relation for comparison with the predicted relation. Hence, for the current consistency checks, we have used the following single regression relation for ETGs: $M_{BH} \propto M_{*,sph}^{1.27 \pm 0.07}$.

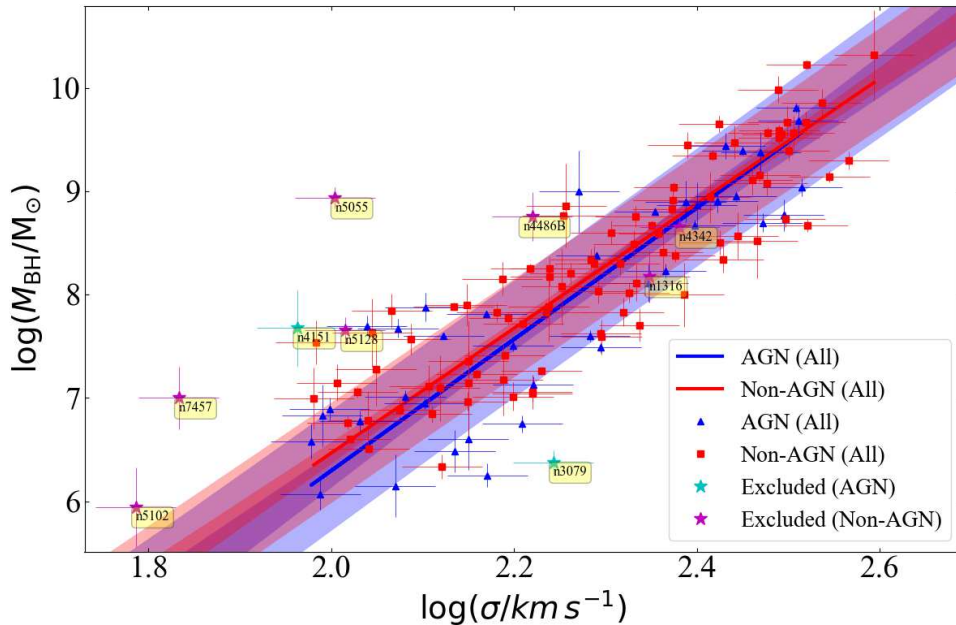


Figure 11. Black hole mass versus velocity dispersion followed by galaxies hosting AGN and galaxies without AGN.

Using $M_{BH} \propto \sigma^{8.54 \pm 0.33}$ (Equation 6) for our core-Sérsic galaxies, all of which are ETGs, and the $M_{BH}-M_{*,gal}$ (and $M_{BH}-M_{*,sph}$) relations for the ETGs from Sahu et al. (2019), we expect the relations $M_{*,gal} \propto \sigma^{5.17 \pm 0.73}$ and $M_{*,sph} \propto \sigma^{6.72 \pm 0.92}$. These two relations are found to be consistent with the directly derived relations $M_{*,gal} \propto \sigma^{6.07 \pm 1.04}$ and $M_{*,sph} \propto \sigma^{6.41 \pm 1.31}$, obtained for our core-Sérsic galaxies using the BCES(BISECTOR) regression.

Using the single regression relation for all (ETG+LTG) Sérsic galaxies $M_{BH} \propto \sigma^{5.86 \pm 0.33}$ (Equation 5), and the $M_{BH}-M_{*,gal}$ (and $M_{BH}-M_{*,sph}$) relations for the ETGs from Sahu et al. (2019), Sérsic ETGs are expected to follow $M_{*,gal} \propto \sigma^{3.55 \pm 0.31}$ and $M_{*,sph} \propto \sigma^{4.61 \pm 0.36}$. These are consistent with the directly-derived relations $M_{*,gal} \propto \sigma^{2.93 \pm 0.35}$ and $M_{*,sph} \propto \sigma^{3.88 \pm 0.45}$ using the BCES(BISECTOR) regression.

Similarly, for Sérsic LTGs, using our Equation 5 and the $M_{BH}-M_{*,gal}$ (and $M_{BH}-M_{*,sph}$) relations from Davis et al. (2019), we predict the relations $M_{*,gal} \propto \sigma^{1.91 \pm 0.45}$ and $M_{*,sph} \propto \sigma^{2.71 \pm 0.43}$, which are consistent with the directly-derived relations $M_{*,gal} \propto \sigma^{2.00 \pm 0.34}$ and $M_{*,sph} \propto \sigma^{2.78 \pm 0.59}$. In the same way, the relations for all the other subcategories, as described in the above subsections, have been found to be internally consistent. In the following sections, we turn our attention to matters of external consistency.

5. THE $L-\sigma$ DIAGRAM

For half a century, astronomers have been studying the correlation between the luminosity of a galaxy and the velocity dispersion of the stars in it (Minkowski 1962). Faber & Jackson (1976) provided the first scaling relation $L_B \propto \sigma^4$, aka the “Faber-Jackson relation”, for ETGs, using their measurements of the velocity dispersion for 25 ETGs. However, with the increase in the number of reliable measurements at bright and faint luminosities, astronomers found different power-laws when using different samples. Schechter (1980) reported $L_B \propto \sigma^{5.4 \pm 1.0}$ using a sample of 32 mainly bright elliptical galaxies. Malumuth & Kirshner (1981) found that Brightest Cluster Member (BCM) galaxies do not follow the $L_V \propto \sigma^{3.8 \pm 0.6}$ relation which they found for the (relatively low-luminosity) elliptical galaxies in their sample; they noticed that the BCM galaxies have higher velocity dispersions than predicted by the relation for their (low-mass) elliptical galaxies. Around the same time, Tonry (1981) reported a relation with a shallower slope, $L_B \propto \sigma^{3.2 \pm 0.2}$, upon including faint elliptical galaxies, suggesting that a bent or curved $L-\sigma$ relation describes ETGs (see also Binney 1982; Farouki et al. 1983). For dwarf elliptical galaxies, observations revealed a power-law slope of ≈ 2 , further emphasizing the bend in the $L-\sigma$ relation, with the bend-point at $\mathfrak{M}_B \approx -20.5$ mag in the Vega magnitude system (Davies et al. 1983; Held et al. 1992; de Rijcke et al. 2005; Matković & Guzmán 2005).

Kormendy & Bender (2013) subsequently used elliptical galaxies from the data-set of Lauer et al. (2007), with some modifications, and reported a steep $L \propto \sigma^8$

relation for the core (core-Sérsic) elliptical galaxies, and $L \propto \sigma^4$ for the core-less (Sérsic) elliptical galaxies. Although they specifically mention the use of a symmetric least squares regression routine from Tremaine et al. (2002), they only performed a least squares minimization of the offsets in the σ -direction over \mathfrak{M}_V which produces a steep L - σ slope. The modified FITEXY routine from (Tremaine et al. 2002) does not directly provide a symmetric regression line: one first needs to obtain the $(Y|X)$ and $(X|Y)$ regression lines using this routine, and then find the bisector line (see our Section 3). For the data used by Kormendy & Bender (2013), the symmetric application of the modified FITEXY regression routine gives $L_V \propto \sigma^{4.39 \pm 0.61}$ for the core-Sérsic elliptical galaxies, and $L_V \propto \sigma^{2.98 \pm 0.31}$ for the Sérsic elliptical galaxies.

Graham & Soria (2019) suggest that it is worth exploring if the two distinct relations in the L - σ diagram, may be due to elliptical galaxies at the luminous end and ETGs with a disk at the intermediate and faint end of the relation, instead of core-Sérsic and Sérsic galaxies. Here we re-investigated the L - σ relation using the V-band data from Lauer et al. (2007) and our $3.6 \mu\text{m}$ data.

We have used all of the ETGs (for which σ is available) from Lauer et al. (2007) to construct the V-band \mathfrak{M}_V - σ relations⁶, except for the M32-type compact elliptical galaxies which can bias the relation (Graham & Soria 2019, see their Figure 11). We updated the core designation for the galaxies NGC 4458, NGC 4473, NGC 4478, and NGC 4482 according to Kormendy et al. (2009, their Table 1), and the core designation of NGC 524, NGC 821, NGC 1374, NGC 3607, and NGC 5576 according to our Table 1. We also changed the designation of NGC 4552 from core-Sérsic to Sérsic following Bonfini et al. (2018), which claims that the apparent core detected in this galaxy is because of the dust rings obstructing the light from the galactic center.

We used a constant 10% error on the velocity dispersion, and a 0.2 mag uncertainty on the absolute magnitude, i.e., a 20% error in the luminosity. Before performing the regression on the updated data-set, we checked to see if any single galaxies might bias the underlying relation defined by the bulk of the sample. We excluded the galaxies NGC 1399, NGC 4291, NGC 4467, NGC 4482, NGC 4486B and NGC 4889 from our regressions. We exclude the Sérsic galaxies NGC 4467 and NGC 4482 as

they appear to have an underestimated velocity dispersion, while the core-Sérsic galaxy NGC 4889, appears to have a low V-band magnitude; this makes these galaxies have significant leverage on the slope of the relations. NGC 4486B, as explained in our Section ?? as well, is tidally stripped of its stellar mass. NGC 1399 and NGC 4291, as shown in Figure 12, are also significant outliers and may have a torque effect on the best-fit line for the core-Sérsic galaxies; hence we exclude them in order to obtain a more robust regression.

Figure 12 shows the V-band magnitude versus the velocity dispersion relation for Sérsic and core-Sérsic ETGs from the updated sample of Lauer et al. (2007). We obtain the bend-point at $\mathfrak{M}_V = -20.7$ mag (Vega), with core-Sérsic ETGs defining the relation

$$\log(L_V) = (5.02 \pm 0.59) \log\left(\frac{\sigma}{200 \text{ km s}^{-1}}\right) + (8.54 \pm 0.07), \quad (14)$$

with $\Delta_{rms|L_V} = 0.35$ dex in the $\log L_V$ -direction, and Sérsic ETGs defining a shallower relation given by,

$$\log(L_V) = (2.46 \pm 0.18) \log\left(\frac{\sigma}{200 \text{ km s}^{-1}}\right) + (8.40 \pm 0.04), \quad (15)$$

with $\Delta_{rms|L_V} = 0.32$ dex, obtained using the BCES(BISECTOR) regression.

Using our $3.6 \mu\text{m}$ data for ETGs, we recover the bend in the L - σ relation (Figure 13). For this case, apart from ETG exclusions mentioned in Section ??, we also exclude the core-Sérsic ETG NGC 4291 (shown in Figure 13 by a magenta colored star), as it is a substantial outlier and may bias the best-fit line. Our core-Sérsic galaxies follow the relation

$$\log(L_{3.6\mu\text{m}}) = (5.16 \pm 0.52) \log\left(\frac{\sigma}{200 \text{ km s}^{-1}}\right) + (8.56 \pm 0.08), \quad (16)$$

with $\Delta_{rms|L_{3.6\mu\text{m}}} = 0.19$ dex (in the $\log L_{3.6\mu\text{m}}$ -direction) and Sérsic galaxies follow the shallower relation,

$$\log(L_{3.6\mu\text{m}}) = (3.07 \pm 0.43) \log\left(\frac{\sigma}{200 \text{ km s}^{-1}}\right) + (8.70 \pm 0.07), \quad (17)$$

with $\Delta_{rms|L_{3.6\mu\text{m}}} = 0.38$ dex.

The different exponent of the relations $L_B \propto \sigma^{2.0}$ (Graham & Soria 2019), $L_V \propto \sigma^{2.5}$ (Figure 12), and $L_{3.6\mu\text{m}} \propto \sigma^{3.1}$ (Figure 13) followed by Sérsic ETGs in different wavelength bands is consistent with the fact that they also follow a color-magnitude relation. Moreover, core-Sérsic ETGs have roughly a constant color, suggesting similar slopes of the L - σ relation for

⁶ Kormendy & Bender (2013) heavily pruned the data sample from Lauer et al. (2007) by excluding many dwarf ETGs which define the low-mass slope, and some lenticular galaxies but not others (see Graham 2019b).

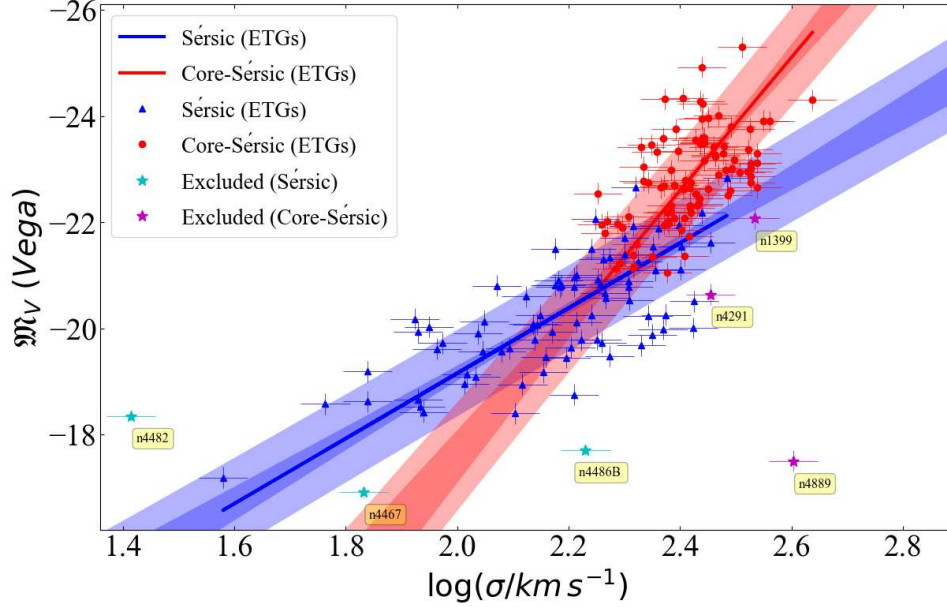


Figure 12. V-band magnitude versus velocity dispersion diagram for Sérsic and core-Sérsic ETGs taken from the sample of Lauer et al. (2007). The BCES(BISECTOR) regression provides the relations $L_V \propto \sigma^{2.46 \pm 0.18}$ (Equation 15) and $L_V \propto \sigma^{5.02 \pm 0.59}$ (Equation 14) for Sérsic and core-Sérsic ETGs, respectively. This diagram suggests a broken $L-\sigma$ relation with the bend point $\mathfrak{M}_V \approx -20.7$ mag (Vega).

all wavelength bands. The observed $L-\sigma$ relations for core-Sérsic ETGs in different bands, i.e., $L_B \propto \sigma^{4-6}$ (Graham & Soria 2019), $L_V \propto \sigma^{5.0}$ (Figure 12), and $L_{3.6\mu\text{m}} \propto \sigma^{5.2}$ (Figure 13), are consistent as expected.

In the $3.6\mu\text{m}$ magnitude ($\mathfrak{M}_{3.6\mu\text{m}}$) versus velocity dispersion diagram, we observe the bend-point at $\mathfrak{M}_{3.6\mu\text{m}} \approx -22.3$ mag in the AB magnitude system, which is $\mathfrak{M}_{3.6\mu\text{m}} \approx -25.1$ mag in the Vega magnitude system. Assuming a $B - 3.6\mu\text{m}$ color of ~ 5 (based on $B - K \approx 4$ and $K - 3.6\mu\text{m} \approx 1$), it seems to be consistent with the bend-point reported by previous studies at $\mathfrak{M}_B \approx -20.5$ mag (Graham & Soria 2019), $\mathfrak{M}_V \approx -21$ mag (Lauer et al. 2007), and $\mathfrak{M}_R \approx -22.17$ mag (Matković & Guzmán 2005).

In Sahu et al. (2019), we found that Sérsic and core-Sérsic ETGs follow the same $M_{BH} \propto M_{*,gal}^{1.65 \pm 0.11}$ relation. As the majority of our galaxy data in Sahu et al. (2019) and in this paper is in the $3.6\mu\text{m}$, using the relations $M_{BH} \propto \sigma^{5.14 \pm 0.37}$ for Sérsic ETGs (Equation 4) and $M_{BH} \propto \sigma^{8.54 \pm 1.07}$ for core-Sérsic galaxies (Equation 6), all of which are ETGs, we expect $M_{*,gal} \propto \sigma^{3.11 \pm 0.30}$ and $M_{*,gal} \propto \sigma^{5.17 \pm 0.73}$ for our early-type Sérsic and core-Sérsic galaxies, respectively. These two expected relation are consistent with what we have obtained (Equations 16 and 17, respectively) given that a stellar mass-to-light ratio of 0.6 (Meidt et al. 2014) was used for $3.6\mu\text{m}$ data in Sahu et al. (2019).

We have also plotted and performed regressions on our LTGs, in the $L_{3.6\mu\text{m}}-\sigma$ diagram, as shown in Figure 14.

In addition to the LTGs excluded for our $M_{BH}-\sigma$ relations as mentioned in Section ??, we also exclude the LTGs NGC 1300 and NGC 2974, as they are considerable outliers and could bias the relation. LTGs follow the relation

$$\log(L_{3.6\mu\text{m}}) = (2.55 \pm 0.38) \log\left(\frac{\sigma}{200 \text{ km s}^{-1}}\right) + (9.00 \pm 0.08), \quad (18)$$

with $\Delta_{rms|L_{3.6\mu\text{m}}} = 0.17$ dex, consistent with the expected $M_{*,gal} \propto \sigma^{2.03 \pm 0.51}$ relation, derived from the relations $M_{BH} \propto M_{*,gal}^{3.05 \pm 0.70}$ (Davis et al. 2019) and $M_{BH} \propto \sigma^{6.19 \pm 0.65}$ (Equation 2). The slope of the $L-\sigma$ relation that we derived for the LTGs, is also consistent with the B-band slope of 2.13 reported by Graham et al. (2019, see their Figure 7).

6. SELECTION BIAS

The lack of directly measured low-mass SMBHs due to the technological limitations to resolve their spheres-of-influence poses a possible selection bias on the black hole mass scaling relations. In the past, several studies have discussed the consequences and possible solutions of this sample selection bias (e.g., Batcheldor 2010; Graham et al. 2011; Shankar et al. 2016).

Batcheldor (2010) obtained an artificial $M_{BH}-\sigma$ relation using simulated random M_{BH} and σ data, selected through the constraint of a best available resolution limit of $0''.1$ attainable from the *Hubble Space*

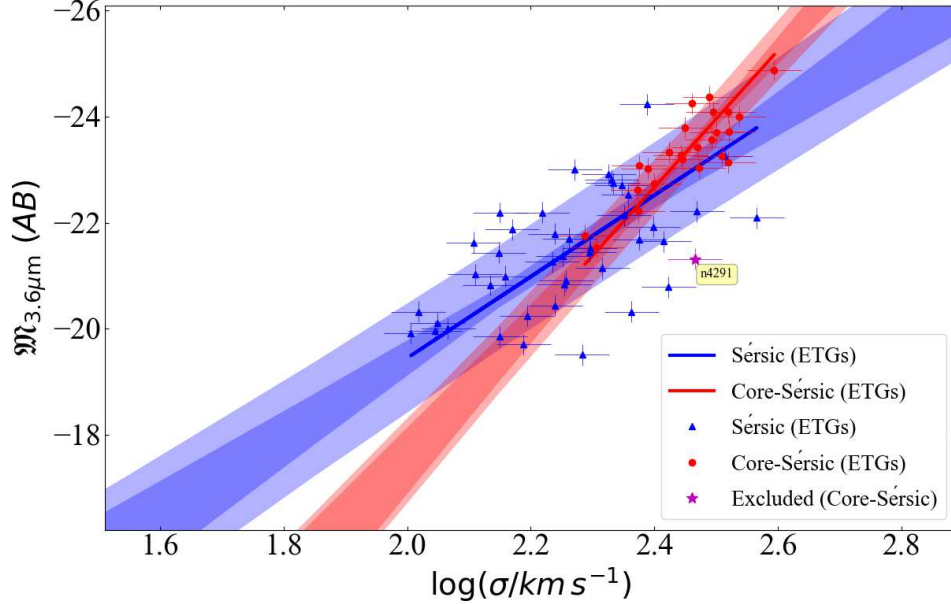


Figure 13. $3.6\ \mu\text{m}$ absolute magnitude versus velocity dispersion for the Sérsic and core-Sérsic ETGs in our sample. We find the bend in the relation at $M_{3.6\mu\text{m}} \approx -22.3$ mag (AB) with Sérsic and core-Sérsic galaxies following the best-fit lines $L_{3.6\mu\text{m}} \propto \sigma^{3.07 \pm 0.43}$ (Equation 17) and $L_{3.6\mu\text{m}} \propto \sigma^{5.16 \pm 0.52}$ (Equation 16), respectively. The color-magnitude relation for Sérsic ETGs explains the different slope of $\sim 2.46 \pm 0.18$ in Figure 12 for the L_V - σ relation.

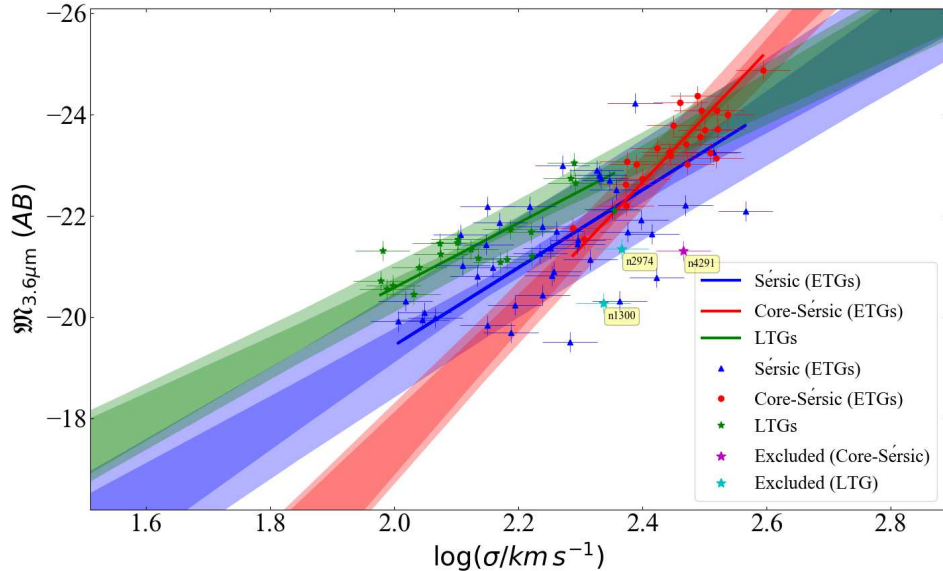


Figure 14. Similar to Figure 13 but including LTGs (spirals). All the spirals in our sample are Sérsic galaxies, and they also seem to define a tight correlation in the L - σ diagram (Equation 18).

Telescope (*HST*), for a maximum distance of 100 Mpc. The fake data produced the relation $\log(M_{BH}/M_{\odot}) = (4.0 \pm 0.3) \log(\sigma/200 \text{ km s}^{-1}) + (8.3 \pm 0.2)$, which was nearly consistent with the then observed $M_{BH}-\sigma$ relation of Gültekin et al. (2009). Batcheldor (2010) highlighted a crucial point for assessing the credibility of the observed black hole scaling relations. However, his relation with a slope of around 4 is lower than the steeper $M_{BH}-\sigma$ relations based on larger samples of dynamically measured M_{BH} data (Graham et al. 2011; McConnell & Ma 2013; Graham & Scott 2013; Savorgnan & Graham 2015; Sabra et al. 2015). It may be insightful to revisit this bias allowing for the range of sub 0'1 data now available, however, this is beyond the scope of the current investigation.

Shankar et al. (2016) claim that galaxies which host a directly measured central SMBH have a higher velocity dispersion in comparison to other galaxies of similar stellar mass but without a direct SMBH measurement. Their claim is based on the offset they observed in the velocity dispersion versus galaxy stellar mass diagram ($\sigma-M_{STAR}$, their Figure-1), between several samples of local ETGs with dynamically measured SMBH masses and a larger data-set of galaxies from Data Release-7 of the Sloan Digital Sky Survey (SDSS, York et al. 2000; Abazajian et al. 2009).

Shankar et al. (2016) suggest that the offset they obtain is a consequence of a sample selection effect due to the lack of dynamically-measured low-mass black holes, for which it is not possible to resolve their spheres-of-influence due to technological limitations. They performed the comparison with the data from four different observational studies and provided a unified conclusion that galaxies hosting a directly-measured SMBH are offset in the $\sigma-M_{*,gal}$ relation, such that they have a higher σ relative to other similar mass galaxies. However, this is not completely true for all the data-sets they used and all of the galaxy stellar mass range in their plots. In their Figure-1, a significant number of data points from Savorgnan et al. (2016) overlap within the grey $\pm 1\sigma$ dispersion bands around the mean curve of the SDSS data, especially in the high-mass range ($11 \lesssim \log(M_{*,gal}/M_{\odot}) \lesssim 12$).

Interestingly, as described in Section 4, we have found that Sérsic and core-Sérsic ETGs follow two distinct $M_{*,gal}-\sigma$ relations, consistent with Sérsic and core-Sérsic ETGs following two different $M_{BH}-\sigma$ relations (Section 3.2), but a single $M_{BH}-M_{*,gal}$ relation (Sahu et al. 2019). Thus, we have a bent relation in the $\sigma-M_{*,gal}$ diagram for Sérsic and core-Sérsic ETGs as shown in the left panel of Figure 15. The mean (black) curve from Shankar et al. (2016) lays within the

$\pm 1\sigma$ scatter of the two relations followed by our Sérsic and core-Sérsic ETGs with directly-measured black hole masses, but outside of the more relevant darker (red and blue) bands denoting the $\pm 1\sigma$ uncertainty on the $\sigma-M_{*,gal}$ relations for ETGs with directly-measured black hole masses.

Upon inclusion of our LTGs (in the right panel of Figure 15), all of which are Sérsic galaxies, along with the (core-Sérsic and Sérsic) ETGs, we find that at the low-mass range ($10 \lesssim \log(M_{*,gal}/M_{\odot}) \lesssim 11$), their (black) curve resides between the two relations followed by our Sérsic ETGs (blue line) and LTGs (green line). This suggests that their galaxy sample of ETGs may contain LTGs which (partly) cause the offset.

In Shankar et al. (2016), the criteria for selecting only ETGs out of the exhaustive SDSS data-set was based upon having a probability of greater than 0.8 for a galaxy being an E- or S0- type ($P(E - S0) \geq 0.8$). From the probabilities of galaxy types made available by Meert et al. (2015), we calculated an $\sim 10\%$ contamination by spiral galaxies (LTGs) in their ETG sample. Their best-fit $\sigma-M_{*,gal}$ relation's position in-between the relation followed by our Sérsic ETGs and LTGs (right panel of Figure 15), coupled with their ETG selection criteria based on probability, supports the suspicion that some of the offset is due to spiral galaxy contamination in their SDSS ETG sample.

7. IMPLICATIONS AND CONCLUSIONS

Our $M_{BH}-\sigma$ (and $M_{BH}-M_{*,gal}$, and $M_{BH}-M_{*,sph}$) relations hold insights for theoretical studies into the co-evolution of black holes with their host galaxies (Heckman & Best 2014), and its impact on galaxy properties (Volonteri & Ciotti 2013), AGN feedback (Marconi et al. 2008), the connection between black hole growth and star formation rates, which further depends on galaxy morphology (Calvi et al. 2018), and so on. Black hole mass scaling relations are also used to determine virial f -factors, for calculating AGN (black hole) masses (e.g., Onken et al. 2004; Graham et al. 2011; Bennert et al. 2011; Bentz & Katz 2015; Yu et al. 2019). Our $M_{BH}-\sigma$ relation due to Sérsic and core-Sérsic galaxies can be used to improve the virial f -factor based on galaxy core-type.

The new black hole mass scaling relations can be used to estimate the black hole masses of other galaxies using their easily measured properties, i.e., their galaxy stellar mass, spheroid/bulge stellar mass, or stellar velocity dispersion. These scaling relations, based on high resolution images of local galaxies ($z \sim 0$), work as a benchmark for studies attempting to determine the evolution of the $M_{BH}-\sigma$ (or $M_{BH}-M_{*,gal}$ and $M_{BH}-M_{*,sph}$) re-

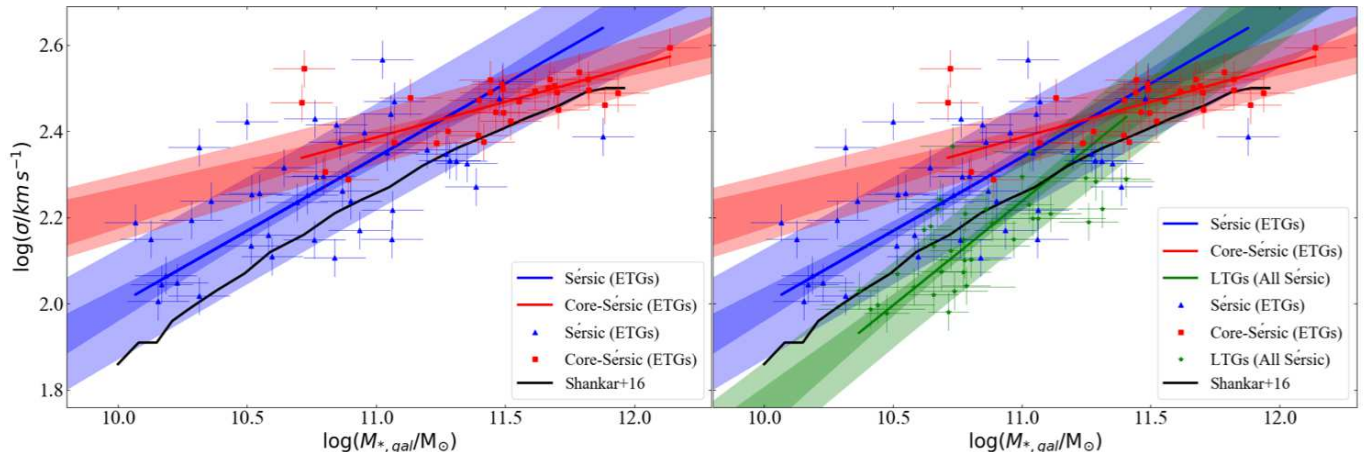


Figure 15. Velocity dispersion versus total galaxy stellar mass relation for Sérsic and core-Sérsic ETGs in the left panel, and also including LTGs (which are all Sérsic) in the right panel, along with the mean best-fit σ - $M_{*,gal}$ (black) curve for SDSS data from Shankar et al. (2016, their Figure 1 where they used M_{STAR} for the total galaxy stellar mass). The left panel shows that their best-fit curve falls within the $\pm 1\sigma$ scatter region of the relations followed by our Sérsic and core-Sérsic ETGs. The offset is possibly due to spiral contamination in their ETGs sample. The second panel shows that the black curve falls between the best-fit lines for Sérsic ETGs and LTGs, especially at low-mass end, suggesting that their so-called ETGs sample might be contaminated with LTGs.

lations (Bennert et al. 2011; Hiner 2012; Sexton et al. 2019). Moreover, given the different scaling relations based on the galaxy sub-morphologies, care should be taken in regard to the galaxy types present in one’s sample.

Our scaling relations can be used to estimate black hole masses for a large data-set of galaxies to obtain a black hole mass function of the local universe (Driver 2006; Driver et al. 2007). This can be used to improve the predictions of the amplitude and frequency of ground-based detections of long-wavelength gravitational waves, produced by merging SMBHs, using pulsar timing arrays (Shannon et al. 2015; Hobbs & Dai 2017) and also MeerKAT (Jonas 2007). Furthermore, these scaling relations can also be used to constrain the space-based detection of long-wavelength gravitational waves by the Laser Interferometer Space Antenna (LISA, Danzmann 2017), and beyond LISA (bLISA, Baker et al. 2019).

According to Zubovas & King (2019), the low-spinning SMBHs are more massive and tend to follow a steeper M_{BH} - σ relation. Thus, the two relations in the M_{BH} - σ diagram, i.e., the steeper $M_{BH} \propto \sigma^{8.54 \pm 1.07}$ relation (Equation 6) followed by core-Sérsic galaxies and the shallower relation $M_{BH} \propto \sigma^{5.86 \pm 0.33}$ (Equation 5) followed by Sérsic galaxies, also provide a measure of the spin of a black hole.

Using the reduced sample of 130 galaxies with updated black hole masses and central stellar velocity dispersions, our work reveals sub-structures in the M_{BH} - σ diagram due to both: galaxies with and without a core,

and galaxies with and without a disk, the latter being a consequence of the former. Our previous galaxy decompositions (Savorgnan & Graham 2016; Davis et al. 2019; Sahu et al. 2019) have enabled us to accurately identify various structural components, such as intermediate or extended disks, bars, and partially-depleted stellar cores. This allowed us to search for substructures in the M_{BH} - σ diagram, based on galaxy morphology, and also enabled us to clarify the situation regarding offset barred galaxies found in previous works.

We performed and reported both symmetric BCES(BISECTOR) and asymmetric BCES($Y|X$) and BCES($X|Y$) regressions. The best-fit line obtained from the symmetric BCES(BISECTOR) regression is preferred because we are looking for a fundamental relation between two quantities (Feigelson & Babu 1992; Novak et al. 2006). For all our relations, we also obtained a symmetric (bisector) regression line using the MPFITEXY (modified FITEXY) routine. All are consistent with the corresponding BCES(BISECTOR) best-fit lines within the $\pm 1\sigma$ limits of the slopes and intercepts.

Our main results can be summarized as follows:

- The consistency between the best-fit lines for ETGs and LTGs in the M_{BH} versus σ diagram (Figure 1), suggests that ETGs and LTGs follow the same $M_{BH} \propto \sigma^{6.19 \pm 0.27}$ relation with a total scatter of $\Delta_{rms|BH} = 0.50$ dex, obtained using a single regression on the total sample (Equation 3). However, this result depends on the galaxy sam-

ple and is somewhat misleading or limited. It is a fusion of substructures caused by (massive) core-Sérsic and (low-mass) Sérsic galaxies following two different $M_{BH}-\sigma$ relations.

- Core-Sérsic galaxies define the relation $M_{BH} \propto \sigma^{8.54 \pm 1.07}$ (Equation 6) and Sérsic galaxies define the relation $M_{BH} \propto \sigma^{5.86 \pm 0.33}$ (Equation 5), with $\Delta_{rms|BH} = 0.47$ dex and $\Delta_{rms|BH} = 0.51$ dex, respectively. The inconsistency between the slopes of these two relations suggests a “broken” or “bent” $M_{BH}-\sigma$ relation. The two lines intersect at $\sigma \approx 255 \text{ km s}^{-1}$ in Figure 4 .
- We also obtain a bend in the $M_{BH}-\sigma$ diagram upon dividing our sample into galaxies with and without a stellar disk (Figures 5 and 6). However, this is likely because most of the elliptical ETGs are massive core-Sérsic galaxies, while most of the galaxies with a disk (ES, S0, and Sp-types) are Sérsic galaxies.
- We do not find any offset between the slope or intercept of the best-fit lines for barred and non-barred galaxies (Figures 7 and 8). We reveal that some previous studies noticed an offset in the intercepts between the $M_{BH}-\sigma$ relations for barred and non-barred galaxies partly because they relied on incomplete bar morphologies for several galaxies which failed to identify weak bars. Our previous image analysis improved upon this situation, and now in our current larger sample we also have new galaxies with bars. Given that bars are known to elevate the velocity dispersion (Hartmann et al. 2014), this result begs further investigation, possibly folding in disc inclination, bar orientation to our line-of-sight, and rotational velocity.
- Galaxies with and without an AGN follow consistent relations in the $M_{BH}-\sigma$ diagram (Figure 11). Hence, the $M_{BH}-\sigma$ relations defined by Sérsic and core-Sérsic galaxies should be valid for a galaxy irrespective of whether or not its nucleus is active.
- Analyzing the $L-\sigma$ relation, based on updated V-band data from Lauer et al. (2007), our $3.6 \mu\text{m}$ data from Spitzer, and previously reported $L-\sigma$ relations using B- and R-bands, we investigate the $L-\sigma$ relation (Figure 12 and 13). We find that the relation between the luminosity of a galaxy and its central stellar velocity dispersion is bent due to core-Sérsic and Sérsic galaxies, analogous and consistent with the bend found in the $M_{BH}-\sigma$ relation and the $L-\mu_0$ relation (Graham & Guzmán 2003). Core-Sérsic galaxies follow $L_V \propto \sigma^{5.02 \pm 0.59}$ and $L_{3.6 \mu\text{m}} \propto \sigma^{5.16 \pm 0.52}$ (Equations 14 and 16), whereas Sérsic galaxies follow $L_V \propto \sigma^{2.46 \pm 0.18}$ and $L_{3.6 \mu\text{m}} \propto \sigma^{3.07 \pm 0.43}$ (Equations 15 and 17). The bend-point is consistent in the B-, V-, and $3.6 \mu\text{m}$ bands.
- The LTGs in our sample follow $L_{3.6 \mu\text{m}} \propto \sigma^{2.55 \pm 0.38}$ (Equation 18), and all the $L_{3.6 \mu\text{m}}-\sigma$ relations are internally consistent with our $M_{BH}-\sigma$, and $M_{BH}-M_{*,gal}$ relations from (Sahu et al. 2019).

ACKNOWLEDGMENTS

This research was conducted with the Australian Research Council Centre of Excellence for Gravitational Wave Discovery (OzGrav), through project number CE170100004. AWG was supported under the Australian Research Council’s funding scheme DP17012923. This work has made use of the NASA/IPAC Infrared Science Archive and the NASA/IPAC Extragalactic Database (NED). This research has also made use of the Two Micron All Sky Survey and Sloan Digital Sky Survey database. We also acknowledge the use of the HYPERLEDA database <http://leda.univ-lyon1.fr>.

REFERENCES

- Abazajian, K. N., Adelman-McCarthy, J. K., Agüeros, M. A., et al. 2009, ApJS, 182, 543, doi: [10.1088/0067-0049/182/2/543](https://doi.org/10.1088/0067-0049/182/2/543)
- Akritas, M. G., & Bershady, M. A. 1996, ApJ, 470, 706, doi: [10.1086/177901](https://doi.org/10.1086/177901)
- Baker, J., Barke, S. F., Bender, P. L., et al. 2019, arXiv e-prints, arXiv:1907.11305. <https://arxiv.org/abs/1907.11305>
- Batcheldor, D. 2010, ApJL, 711, L108, doi: [10.1088/2041-8205/711/2/L108](https://doi.org/10.1088/2041-8205/711/2/L108)
- Batcheldor, D., Robinson, A., Axon, D. J., Perlman, E. S., & Merritt, D. 2010, ApJ, 717, L6, doi: [10.1088/2041-8205/717/1/L6](https://doi.org/10.1088/2041-8205/717/1/L6)
- Bedregal, A. G., Aragón-Salamanca, A., & Merrifield, M. R. 2006, MNRAS, 373, 1125, doi: [10.1111/j.1365-2966.2006.11031.x](https://doi.org/10.1111/j.1365-2966.2006.11031.x)

- Begelman, M. C., Blandford, R. D., & Rees, M. J. 1980, *Nature*, 287, 307, doi: [10.1038/287307a0](https://doi.org/10.1038/287307a0)
- Bellstedt, S., Graham, A. W., Forbes, D. A., et al. 2017, *MNRAS*, 470, 1321, doi: [10.1093/mnras/stx1348](https://doi.org/10.1093/mnras/stx1348)
- Bennert, V. N., Auger, M. W., Treu, T., Woo, J.-H., & Malkan, M. A. 2011, *ApJ*, 726, 59, doi: [10.1088/0004-637X/726/2/59](https://doi.org/10.1088/0004-637X/726/2/59)
- Bentz, M. C., & Katz, S. 2015, *PASP*, 127, 67, doi: [10.1086/679601](https://doi.org/10.1086/679601)
- Binney, J. 1982, *ARA&A*, 20, 399, doi: [10.1146/annurev.aa.20.090182.002151](https://doi.org/10.1146/annurev.aa.20.090182.002151)
- Blom, C., Forbes, D. A., Foster, C., Romanowsky, A. J., & Brodie, J. P. 2014, *MNRAS*, 439, 2420, doi: [10.1093/mnras/stu095](https://doi.org/10.1093/mnras/stu095)
- Boizelle, B. D., Barth, A. J., Walsh, J. L., et al. 2019, arXiv e-prints, arXiv:1906.06267, <https://arxiv.org/abs/1906.06267>
- Bonfini, P., González-Martín, O., Fritz, J., et al. 2018, *MNRAS*, 478, 1161, doi: [10.1093/mnras/sty1087](https://doi.org/10.1093/mnras/sty1087)
- Brown, J. S., Valluri, M., Shen, J., & Debattista, V. P. 2013, *ApJ*, 778, 151, doi: [10.1088/0004-637X/778/2/151](https://doi.org/10.1088/0004-637X/778/2/151)
- Calvi, R., Vulcani, B., Poggianti, B. M., et al. 2018, *MNRAS*, 481, 3456, doi: [10.1093/mnras/sty2476](https://doi.org/10.1093/mnras/sty2476)
- Ciotti, L., & van Albada, T. S. 2001, *ApJL*, 552, L13, doi: [10.1086/320260](https://doi.org/10.1086/320260)
- Combes, F., García-Burillo, S., Audibert, A., et al. 2019, *A&A*, 623, A79, doi: [10.1051/0004-6361/201834560](https://doi.org/10.1051/0004-6361/201834560)
- Dalla Bontà, E., Ferrarese, L., Corsini, E. M., et al. 2009, *ApJ*, 690, 537, doi: [10.1088/0004-637X/690/1/537](https://doi.org/10.1088/0004-637X/690/1/537)
- Danzmann, K. 2017, in *Society of Photo-Optical Instrumentation Engineers (SPIE) Conference Series*, Vol. 10566, Proc. SPIE, 1056610, doi: [10.1117/12.2308272](https://doi.org/10.1117/12.2308272)
- Davies, R. L., et al. 1983, *ApJ*, 266, 41, doi: [10.1086/160757](https://doi.org/10.1086/160757)
- Davis, B. L., Graham, A. W., & Cameron, E. 2018, *ApJ*, 869, 113, doi: [10.3847/1538-4357/aae820](https://doi.org/10.3847/1538-4357/aae820)
- Davis, B. L., Graham, A. W., & Cameron, E. 2019, *ApJ*, 873, 85, doi: [10.3847/1538-4357/aaf3b8](https://doi.org/10.3847/1538-4357/aaf3b8)
- de Rijcke, S., Michielsen, D., Dejonghe, H., Zeilinger, W. W., & Hau, G. K. T. 2005, *A&A*, 438, 491, doi: [10.1051/0004-6361:20042213](https://doi.org/10.1051/0004-6361:20042213)
- de Vaucouleurs, G., de Vaucouleurs, A., Corwin, Herold G., J., et al. 1991, *Third Reference Catalogue of Bright Galaxies*
- Driver, S. 2006, in *The Fabulous Destiny of Galaxies: Bridging Past and Present*, 409, <https://arxiv.org/abs/astro-ph/0509704>
- Driver, S. P., Liske, J., & Graham, A. W. 2007, in *Astronomical Society of the Pacific Conference Series*, Vol. 374, *From Stars to Galaxies: Building the Pieces to Build Up the Universe*, ed. A. Vallenari, R. Tantalo, L. Portinari, & A. Moretti, 481, <https://arxiv.org/abs/astro-ph/0701468>
- Dullo, B. T. 2014, in *Astronomical Society of the Pacific Conference Series*, Vol. 480, *Structure and Dynamics of Disk Galaxies*, ed. M. S. Seigar & P. Treuthardt, 75
- Dullo, B. T., & Graham, A. W. 2013, *ApJ*, 768, 36, doi: [10.1088/0004-637X/768/1/36](https://doi.org/10.1088/0004-637X/768/1/36)
- . 2014, *MNRAS*, 444, 2700, doi: [10.1093/mnras/stu1590](https://doi.org/10.1093/mnras/stu1590)
- Event Horizon Telescope Collaboration, Akiyama, K., Alberdi, A., et al. 2019, *ApJ*, 875, L6, doi: [10.3847/2041-8213/ab1141](https://doi.org/10.3847/2041-8213/ab1141)
- Faber, S. M., & Jackson, R. E. 1976, *ApJ*, 204, 668, doi: [10.1086/154215](https://doi.org/10.1086/154215)
- Fabian, A. C. 1999, *MNRAS*, 308, L39, doi: [10.1046/j.1365-8711.1999.03017.x](https://doi.org/10.1046/j.1365-8711.1999.03017.x)
- Farouki, R. T., Shapiro, S. L., & Duncan, M. J. 1983, *ApJ*, 265, 597, doi: [10.1086/160704](https://doi.org/10.1086/160704)
- Feigelson, E. D., & Babu, G. J. 1992, *ApJ*, 397, 55, doi: [10.1086/171766](https://doi.org/10.1086/171766)
- Ferrarese, L., & Ford, H. 2005, *SSRv*, 116, 523, doi: [10.1007/s11214-005-3947-6](https://doi.org/10.1007/s11214-005-3947-6)
- Ferrarese, L., & Merritt, D. 2000, *ApJ*, 539, L9, doi: [10.1086/312838](https://doi.org/10.1086/312838)
- Gebhardt, K., Bender, R., Bower, G., et al. 2000, *ApJ*, 539, L13, doi: [10.1086/312840](https://doi.org/10.1086/312840)
- Graham, A. 2007, in *Bulletin of the American Astronomical Society*, Vol. 39, *American Astronomical Society Meeting Abstracts*, 759
- Graham, A. W. 2008a, *PASA*, 25, 167, doi: [10.1071/AS08013](https://doi.org/10.1071/AS08013)
- . 2008b, *ApJ*, 680, 143, doi: [10.1086/587473](https://doi.org/10.1086/587473)
- Graham, A. W. 2014, in *Astronomical Society of the Pacific Conference Series*, Vol. 480, *Structure and Dynamics of Disk Galaxies*, ed. M. S. Seigar & P. Treuthardt, 185, <https://arxiv.org/abs/1311.7207>
- Graham, A. W. 2016, in *Galactic Bulges*, Vol. 418, 263
- . 2019, *MNRAS*, 1547, doi: [10.1093/mnras/stz1623](https://doi.org/10.1093/mnras/stz1623)
- Graham, A. W., Ciambur, B. C., & Savorgnan, G. A. D. 2016a, *ApJ*, 831, 132, doi: [10.3847/0004-637X/831/2/132](https://doi.org/10.3847/0004-637X/831/2/132)
- Graham, A. W., & Driver, S. P. 2007, *ApJ*, 655, 77, doi: [10.1086/509758](https://doi.org/10.1086/509758)
- Graham, A. W., Durré, M., Savorgnan, G. A. D., et al. 2016b, *ApJ*, 819, 43, doi: [10.3847/0004-637X/819/1/43](https://doi.org/10.3847/0004-637X/819/1/43)
- Graham, A. W., & Guzmán, R. 2003, *AJ*, 125, 2936, doi: [10.1086/374992](https://doi.org/10.1086/374992)

- Graham, A. W., & Scott, N. 2013, *ApJ*, 764, 151, doi: [10.1088/0004-637X/764/2/151](https://doi.org/10.1088/0004-637X/764/2/151)
- Graham, A. W., & Soria, R. 2019, *MNRAS*, 484, 794, doi: [10.1093/mnras/sty3398](https://doi.org/10.1093/mnras/sty3398)
- Graham, A. W., Soria, R., & Davis, B. L. 2019, *MNRAS*, 484, 814, doi: [10.1093/mnras/sty3068](https://doi.org/10.1093/mnras/sty3068)
- Graham, A. W., et al. 2003, *AJ*, 125, 2951, doi: [10.1086/375320](https://doi.org/10.1086/375320)
- . 2011, *MNRAS*, 412, 2211, doi: [10.1111/j.1365-2966.2010.18045.x](https://doi.org/10.1111/j.1365-2966.2010.18045.x)
- Greene, J. E., Peng, C. Y., Kim, M., et al. 2010, *ApJ*, 721, 26, doi: [10.1088/0004-637X/721/1/26](https://doi.org/10.1088/0004-637X/721/1/26)
- Greene, J. E., Seth, A., Kim, M., et al. 2016, *ApJ*, 826, L32, doi: [10.3847/2041-8205/826/2/L32](https://doi.org/10.3847/2041-8205/826/2/L32)
- Gültekin, K., Richstone, D. O., Gebhardt, K., et al. 2009, *ApJ*, 695, 1577, doi: [10.1088/0004-637X/695/2/1577](https://doi.org/10.1088/0004-637X/695/2/1577)
- Hartmann, M., Debattista, V. P., Cole, D. R., et al. 2014, *MNRAS*, 441, 1243, doi: [10.1093/mnras/stu627](https://doi.org/10.1093/mnras/stu627)
- Heckman, T. M., & Best, P. N. 2014, *ARA&A*, 52, 589, doi: [10.1146/annurev-astro-081913-035722](https://doi.org/10.1146/annurev-astro-081913-035722)
- Held, E. V., de Zeeuw, T., Mould, J., & Picard, A. 1992, *AJ*, 103, 851, doi: [10.1086/116106](https://doi.org/10.1086/116106)
- Hilz, M., Naab, T., & Ostriker, J. P. 2013, *MNRAS*, 429, 2924, doi: [10.1093/mnras/sts501](https://doi.org/10.1093/mnras/sts501)
- Hiner, K. D. 2012, PhD thesis, University of California, Riverside
- Hobbs, G., & Dai, S. 2017, arXiv e-prints, arXiv:1707.01615. <https://arxiv.org/abs/1707.01615>
- Hu, J. 2008, *MNRAS*, 386, 2242, doi: [10.1111/j.1365-2966.2008.13195.x](https://doi.org/10.1111/j.1365-2966.2008.13195.x)
- Jonas, J. 2007, in *From Planets to Dark Energy: the Modern Radio Universe*, 7
- King, A., & Nealon, R. 2019, *MNRAS*, 487, 4827, doi: [10.1093/mnras/stz1569](https://doi.org/10.1093/mnras/stz1569)
- King, I. R., & Minkowski, R. 1966, *ApJ*, 143, 1002, doi: [10.1086/148580](https://doi.org/10.1086/148580)
- King, I. R., & Minkowski, R. 1972, in *IAU Symposium, Vol. 44, External Galaxies and Quasi-Stellar Objects*, ed. D. S. Evans, D. Wills, & B. J. Wills, 87
- Kormendy, J., & Bender, R. 2013, *ApJ*, 769, L5, doi: [10.1088/2041-8205/769/1/L5](https://doi.org/10.1088/2041-8205/769/1/L5)
- Kormendy, J., Fisher, D. B., Cornell, M. E., & Bender, R. 2009, *ApJS*, 182, 216, doi: [10.1088/0067-0049/182/1/216](https://doi.org/10.1088/0067-0049/182/1/216)
- Kormendy, J., & Ho, L. C. 2013, *Annual Review of Astronomy and Astrophysics*, 51, 511, doi: [10.1146/annurev-astro-082708-101811](https://doi.org/10.1146/annurev-astro-082708-101811)
- Lauer, T. R., Faber, S. M., Richstone, D., et al. 2007, *ApJ*, 662, 808, doi: [10.1086/518223](https://doi.org/10.1086/518223)
- Liller, M. H. 1966, *ApJ*, 146, 28, doi: [10.1086/148857](https://doi.org/10.1086/148857)
- Malumuth, E. M., & Kirshner, R. P. 1981, *ApJ*, 251, 508, doi: [10.1086/159490](https://doi.org/10.1086/159490)
- Marconi, A., Axon, D. J., Maiolino, R., et al. 2008, *ApJ*, 678, 693, doi: [10.1086/529360](https://doi.org/10.1086/529360)
- Markwardt, C. 2012, MPFIT: Robust non-linear least squares curve fitting. <http://ascl.net/1208.019>
- Matković, A., & Guzmán, R. 2005, *MNRAS*, 362, 289, doi: [10.1111/j.1365-2966.2005.09298.x](https://doi.org/10.1111/j.1365-2966.2005.09298.x)
- McConnell, N. J., & Ma, C.-P. 2013, *ApJ*, 764, 184, doi: [10.1088/0004-637X/764/2/184](https://doi.org/10.1088/0004-637X/764/2/184)
- Meert, A., Vikram, V., & Bernardi, M. 2015, *MNRAS*, 446, 3943, doi: [10.1093/mnras/stu2333](https://doi.org/10.1093/mnras/stu2333)
- Mehrgan, K., Thomas, J., Saglia, R., et al. 2019, arXiv e-prints, arXiv:1907.10608. <https://arxiv.org/abs/1907.10608>
- Meidt, S. E., Schinnerer, E., van de Ven, G., et al. 2014, *ApJ*, 788, 144, doi: [10.1088/0004-637X/788/2/144](https://doi.org/10.1088/0004-637X/788/2/144)
- Merritt, D., & Ferrarese, L. 2001, *ApJ*, 547, 140, doi: [10.1086/318372](https://doi.org/10.1086/318372)
- Merritt, D., & Milosavljević, M. 2005, *Living Reviews in Relativity*, 8, 8, doi: [10.12942/lrr-2005-8](https://doi.org/10.12942/lrr-2005-8)
- Minkowski, R. 1962, in *IAU Symposium, Vol. 15, Problems of Extra-Galactic Research*, ed. G. C. McVittie, 112
- Nemmen, R. S., Georganopoulos, M., Guiriec, S., et al. 2012, *Science*, 338, 1445, doi: [10.1126/science.1227416](https://doi.org/10.1126/science.1227416)
- Nguyen, D. D., Seth, A. C., den Brok, M., et al. 2017, *ApJ*, 836, 237, doi: [10.3847/1538-4357/aa5cb4](https://doi.org/10.3847/1538-4357/aa5cb4)
- Nguyen, D. D., Seth, A. C., Neumayer, N., et al. 2018, *ApJ*, 858, 118, doi: [10.3847/1538-4357/aabe28](https://doi.org/10.3847/1538-4357/aabe28)
- Nguyen, D. D., den Brok, M., Seth, A. C., et al. 2019, arXiv e-prints, arXiv:1902.03813. <https://arxiv.org/abs/1902.03813>
- Novak, G. S., Faber, S. M., & Dekel, A. 2006, *ApJ*, 637, 96, doi: [10.1086/498333](https://doi.org/10.1086/498333)
- Nowak, N., Saglia, R. P., Thomas, J., et al. 2007, *MNRAS*, 379, 909, doi: [10.1111/j.1365-2966.2007.11949.x](https://doi.org/10.1111/j.1365-2966.2007.11949.x)
- Onken, C. A., Ferrarese, L., Merritt, D., et al. 2004, *ApJ*, 615, 645, doi: [10.1086/424655](https://doi.org/10.1086/424655)
- Oser, L., Naab, T., Ostriker, J. P., & Johansson, P. H. 2012, *ApJ*, 744, 63, doi: [10.1088/0004-637X/744/1/63](https://doi.org/10.1088/0004-637X/744/1/63)
- Paturel, G., Petit, C., Prugniel, P., et al. 2003, *A&A*, 412, 45, doi: [10.1051/0004-6361:20031411](https://doi.org/10.1051/0004-6361:20031411)
- Sabra, B. M., Saliba, C., Abi Akl, M., & Chahine, G. 2015, *ApJ*, 803, 5, doi: [10.1088/0004-637X/803/1/5](https://doi.org/10.1088/0004-637X/803/1/5)
- Saglia, R. P., Opitsch, M., Erwin, P., et al. 2016, *ApJ*, 818, 47, doi: [10.3847/0004-637X/818/1/47](https://doi.org/10.3847/0004-637X/818/1/47)
- Sahu, N., Graham, A. W., & Davis, B. L. 2019, *ApJ*, 876, 155, doi: [10.3847/1538-4357/ab0f32](https://doi.org/10.3847/1538-4357/ab0f32)
- Savorgnan, G. A. D., & Graham, A. W. 2015, *MNRAS*, 446, 2330, doi: [10.1093/mnras/stu2259](https://doi.org/10.1093/mnras/stu2259)

- Savorgnan, G. A. D., & Graham, A. W. 2016, *ApJS*, 222, 10, doi: [10.3847/0067-0049/222/1/10](https://doi.org/10.3847/0067-0049/222/1/10)
- Savorgnan, G. A. D., et al. 2016, *ApJ*, 817, 21, doi: [10.3847/0004-637X/817/1/21](https://doi.org/10.3847/0004-637X/817/1/21)
- Schechter, P. L. 1980, *AJ*, 85, 801, doi: [10.1086/112742](https://doi.org/10.1086/112742)
- Sérsic, J. L. 1963, *BAAA*, 6, 41
- Sexton, R. O., Canalizo, G., Hiner, K. D., et al. 2019, *ApJ*, 878, 101, doi: [10.3847/1538-4357/ab21d5](https://doi.org/10.3847/1538-4357/ab21d5)
- Shankar, F., Marulli, F., Bernardi, M., et al. 2013, *MNRAS*, 428, 109, doi: [10.1093/mnras/sts001](https://doi.org/10.1093/mnras/sts001)
- Shankar, F., Bernardi, M., Sheth, R. K., et al. 2016, *MNRAS*, 460, 3119, doi: [10.1093/mnras/stw678](https://doi.org/10.1093/mnras/stw678)
- Shannon, R. M., Ravi, V., Lentati, L. T., et al. 2015, *Science*, 349, 1522, doi: [10.1126/science.aab1910](https://doi.org/10.1126/science.aab1910)
- Silk, J., & Rees, M. J. 1998, *A&A*, 331, L1. <https://arxiv.org/abs/astro-ph/9801013>
- Thater, S., Krajnovic, D., Cappellari, M., et al. 2019, arXiv e-prints. <https://arxiv.org/abs/1902.10175>
- Thomas, J., Ma, C.-P., McConnell, N. J., et al. 2016, *Nature*, 532, 340, doi: [10.1038/nature17197](https://doi.org/10.1038/nature17197)
- Tonry, J. L. 1981, *ApJL*, 251, L1, doi: [10.1086/183681](https://doi.org/10.1086/183681)
- Tremaine, S., Gebhardt, K., Bender, R., et al. 2002, *ApJ*, 574, 740, doi: [10.1086/341002](https://doi.org/10.1086/341002)
- van den Bosch, R. C. E. 2016, *ApJ*, 831, 134, doi: [10.3847/0004-637X/831/2/134](https://doi.org/10.3847/0004-637X/831/2/134)
- Véron-Cetty, M. P., & Véron, P. 2010, *A&A*, 518, A10, doi: [10.1051/0004-6361/201014188](https://doi.org/10.1051/0004-6361/201014188)
- Volonteri, M., & Ciotti, L. 2013, *ApJ*, 768, 29, doi: [10.1088/0004-637X/768/1/29](https://doi.org/10.1088/0004-637X/768/1/29)
- Walsh, J. L., van den Bosch, R. C. E., Gebhardt, K., et al. 2015, *ApJ*, 808, 183, doi: [10.1088/0004-637X/808/2/183](https://doi.org/10.1088/0004-637X/808/2/183)
- Williams, M. J., Bureau, M., & Cappellari, M. 2010, *MNRAS*, 409, 1330, doi: [10.1111/j.1365-2966.2010.17406.x](https://doi.org/10.1111/j.1365-2966.2010.17406.x)
- Woo, J.-H., Schulze, A., Park, D., et al. 2013, *ApJ*, 772, 49, doi: [10.1088/0004-637X/772/1/49](https://doi.org/10.1088/0004-637X/772/1/49)
- York, D. G., Adelman, J., Anderson, John E., J., et al. 2000, *AJ*, 120, 1579, doi: [10.1086/301513](https://doi.org/10.1086/301513)
- Yu, L.-M., Bian, W.-H., Wang, C., Zhao, B.-X., & Ge, X. 2019, *MNRAS*, 488, 1519, doi: [10.1093/mnras/stz1766](https://doi.org/10.1093/mnras/stz1766)
- Zubovas, K., & King, A. R. 2019, arXiv e-prints, arXiv:1908.02630. <https://arxiv.org/abs/1908.02630>

This figure "orcid-ID.png" is available in "png" format from:

<http://arxiv.org/ps/1908.06838v1>